Exploring electricity generation alternatives for Canadian Arctic communities using a multi-objective genetic algorithm approach

Marvin Rhey Quitoras[a,*], Pietro Elia Campana[b], Curran Crawford[a]

[a]*Department of Mechanical Engineering, University of Victoria, PO Box 3055 STN CSC, Victoria, BC V8W 2Y2, Canada*
[b]*School of Business, Society & Engineering, Mälardalen University, Box 883, SE-72123 Västerås, Sweden*

Abstract

Indigenous peoples in the Northern communities of Canada are experiencing some of the worst catastrophic effects of climate change, given the Arctic region is warming twice as fast as the rest of the world. Paradoxically, this increasing temperature can be attributed to fossil fuel-based power generation on which the North is almost totally reliant. At the moment, diesel is the primary source of electricity for majority of Arctic communities. In addition to greenhouse gas and other airborne pollutants, this situation exposes risk of oil spills during fuel transport and storage. Moreover, shipping fuel is expensive and ice roads are harder to maintain as temperatures rise. As a result, Northern governments are burdened by rising fuel prices and increased supply volatility.

In an effort to reduce diesel dependence, the Multi-objective INtegrated Energy System was built in this work to handle the complex trade-offs of designing energy system for an Arctic environment and other remote communities. The tool uses a genetic algorithm to simultaneously minimize levelised cost of energy and fuel consumption of the microgrid system through dynamic simulations. Component submodel simulation results were validated against an industry and academic accepted energy modeling tool. Compared to previous energy modeling platforms, proposed method is novel in considering Pareto front trade-offs between conflicting design objectives to better support practitioners and policy makers. The functionality of the method was demonstrated with a case study on Sachs Harbour, in the Northernmost region of the Northwest Territories. The algorithm selected a fully hybrid wind-solar-battery-diesel system as the most suited technically, economically and environmentally for the community. The robustness of the results was assessed by performing system failure analysis of the model results. Overall, the modeling framework can help decision makers in identifying trade-offs in energy policy to transition the Canadian Arctic and other remote communities towards more sustainable and clean sources of energy.

Highlights

- Robust multi-objective approach to capture complex trade-offs of designing hybrid microgrid energy systems.
- Multiple system configurations are viable relative to the baseline diesel-only scenario for Sachs Harbour.
- Partial dispatch of diesel power implies higher costs.
- The wind resource is able to meet the largest share of demand.
- The optimal hybrid renewable energy system resulted in a 70% cost reduction in the government subsidy.

Keywords: `Arctic environment; Energy model; Microgrid; Renewable energy; Optimization; Genetic algorithm`

*Corresponding author
Email address: `mdquitoras@uvic.ca` (Marvin Rhey Quitoras)

1. Introduction

More than 50 Indigenous remote communities in the Northern territories[1] rely exclusively on fossil fuels, predominantly diesel, as their primary source of electricity [1] as presented in Fig. 1 and Table 1. The communities are exposed to high energy costs and environmental vulnerabilities which are made worse by the changing Arctic environment. According to the Pembina Institute [2], remote communities in Canada collectively consume more than 90 million liters of diesel fuel every year for electricity generation. Out of the total amount, 59 million liters of diesel (Fig. 1) are transported to the North to serve the electricity demand of almost 100,000 Canadians of which 80% are Indigenous.

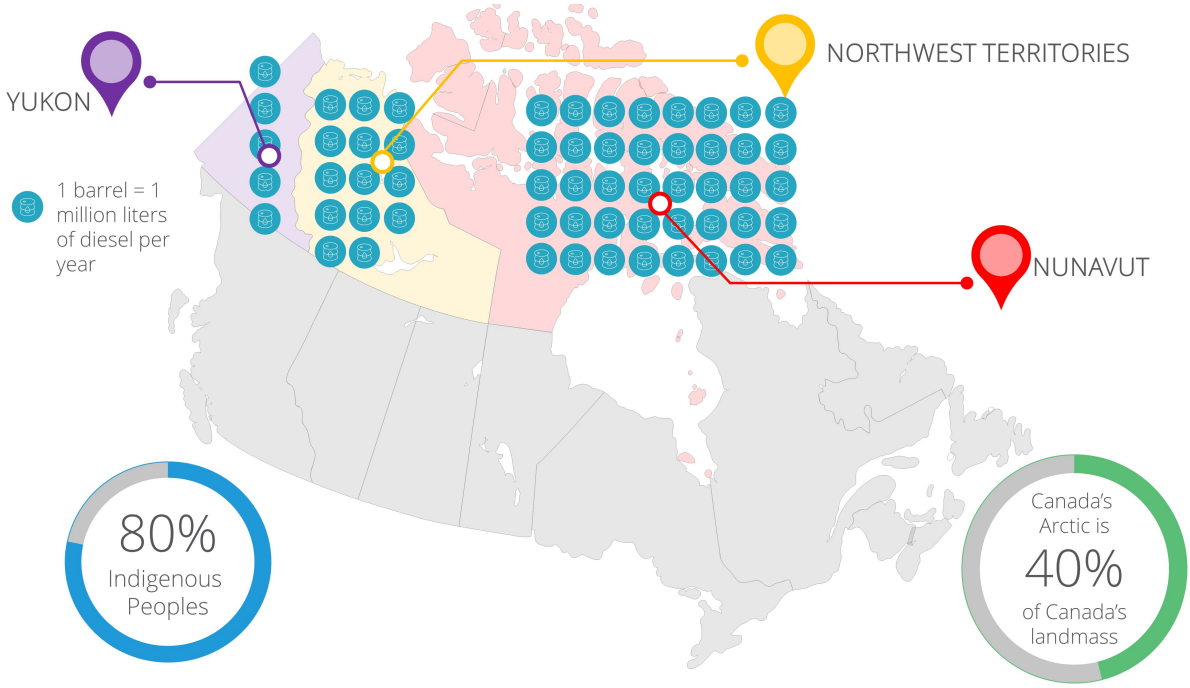

Figure 1: Diesel consumption in Northern territories of Canada. Data Source:Natural Resources Canada [3]

Canada's Arctic covers over 40% of the country's landmass and an area of growing importance internationally [4]. Both the federal and local governments are working together to reduce dependence on diesel as primary source of energy, in large part to their desire to lower emissions and contribute to Canada's commitment to the Paris agreement [5]. Further, decreasing the carbon footprint of the Canadian Arctic will introduce significant impact not just from a country perspective but on a global scale considering the continuous increase of air temperature in Northern latitude communities. The Arctic serves as a massive temperature regulator [6]; its white ice bounces heat back into the space. However, with shrinking Arctic sea ice extent caused by rising air temperatures[2], more heat can infiltrate in the earth's surface and cause dramatic increases in warming in the world.

Protecting Canada's Arctic from oil spills is also one of the concerns of the government to lessen the environmental impact of shipping diesel. A significant amount of fuel never makes it to Northern communities but is lost to fuel spills during fuel transport and storage. According to Environment and Natural Resources Canada [8], roughly 9.1 million liters of diesel has been spilled in Nunavut and NWT since the 1970s, and more than 50% of the leaks are from trucks and storage tanks [9]. Further, the United Nation's International Maritime Organization [10] has stated that a single spill could have devastating and lasting effects on the fragile Arctic marine and coastal environments. The World Wildlife Fund (WWF) has been specifically studying the impact of oil spills in the Arctic [11].

[1]The North in Canada politically refers to the territories of Yukon, Northwest Territories (NWT) and Nunavut; its geographical location as compared to the rest of Canada can be seen in Fig. 1.

[2]The warming of Arctic air temperatures has been caused not only by the increase in greenhouse gas concentra-

To address energy issues, the Northern territories conduct regular Energy Charrettes to bring together representatives and energy experts to tackle challenges and identify energy solutions in the North [12]. Overall, affordability is the most important concern for Indigenous communities. This can be attributed to the high cost of electricity prices in the NWT and Nunavut as shown in Fig. 2(a). Households in these communities pay more than twice the Canadian average electricity price of 12.9 CND cents/kWh. Yukon, on the other hand, pays 13.6 CND cents/kWh which is closer to Canada's average price [13]. Hydropower is the primary source of electricity in Yukon while NWT and Nunavut is primarily diesel (Table 1) making those two regions the focus of the government in shifting to clean sources of energy. In Fig.2(a), the comparative residential electricity prices[3] for the three territories are subsidized by the government. Full costs, based on the first 1000 kWh consumed in winter during 2015, can be seen in Fig. 2(b) [1]. These subsidies have policy implication for every system transition.

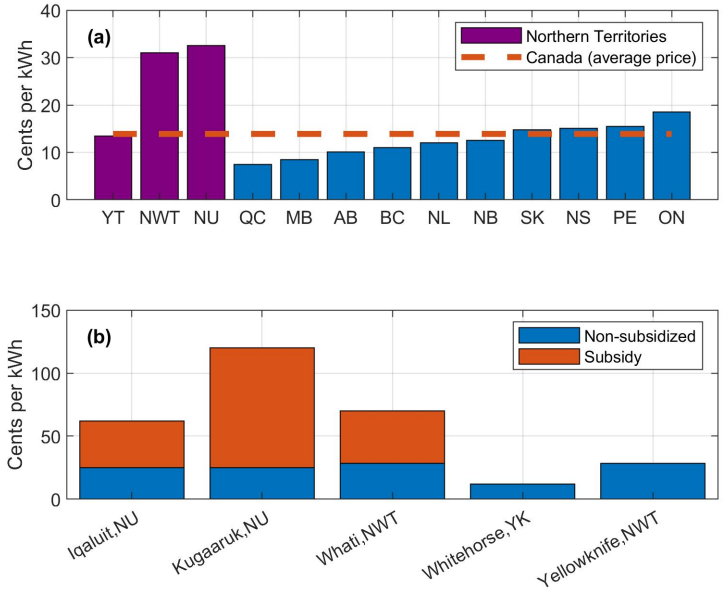

Figure 2: Electricity prices: (a) Representative territorial and provincial residential electricity prices in Canada[13] ; (b) Full costs of residential electricity rates in selected communities in the North [1]

Another significant issue in the North is the method of transporting fuel to the remote communities. Most fuels are shipped from Southern Canada [12] through ice roads and scheduled in bulk. However, this mode of transportation is increasingly unreliable due to climate change resulting in Canada's ice roads freezing later and melting earlier in the year [14]. As a result, most fuels are shipped by small plane, making electricity prices even more expensive, or via boats, which increases the risk of oils spills in the Arctic waters. All of these factors – rising electricity prices, fuel supply volatility, catastrophic warming of the Arctic at twice the global average rate [15], environmental emissions and the likelihood of oil spills – are driving the Canadian government to unfreeze the renewable energy (RE) potential of its Arctic communities.

With this framing in mind, the motivating research question for this study is: ***How can electricity generation alternatives be effectively integrated in the Northern communities of Canada?***

1.1. Energy systems modeling

Energy systems modeling provides a tool to help answer this research question. Biberacher [16] defined a model as a simplified description of reality with the goal of highlighting certain relations

tions (from burning fossil fuels and other sources), but also the deposition of soot ice on Arctic ice [7].

[3]Territorial electricity prices in the graph are based on residential rates in the capital city of each territory: Yellowknife, NWT; Whitehorse, YT and Iqaluit, NU. Provincial prices reflect rates in major cities in each province: Vancouver, BC; Edmonton, AB; Regina, SK; Winnipeg, MB; Toronto, ON; Montréal, QC; Moncton, NB; Halifax, NS; Charlottetown, PE; and, St. John's, NL [13].

and to make the best prediction of future developments possible. In the case of energy systems, Biberacher further described a model as a framework of relations encompassing the technical, economic and social aspects of a system under evaluation. The International Energy Agency also defined energy models as abstractions of reality that simplify the world into "bite sized" pieces in order to fit within certain sets of mathematical methods [17]. They vary in scale from local to global, in sector from electricity or transportation-only, to economy wide. These models are variously capable of simulating, optimizing, forecasting or even backcasting. They can be applied for academic purposes, to guide policy-making, or for investment planning of the private and government sectors.

WWF Canada completed the most recent feasibility study of RE technologies in the North [18]. Over a 25-year planning horizon, their investigations showed that the deployment of hybrid diesel-solar-wind-battery system would economically reduce diesel consumption in Northern remote communities. They used Hybrid Optimization of Multiple Energy Resources (HOMER) software [19] for the pre-feasibility stage of their study and an in-house mathematical optimization model of RE integration based on a long term generation expansion planning approach during the feasibility phase. For both cases, they minimized Net Present Cost (NPC) in order to determine the most feasible configuration of the energy system. HOMER finds the most feasible configuration by applying a full factorial design of experiments and choosing the configuration with the minimum NPC. With its user-friendly interface, HOMER is probably the most widely used software in evaluating feasibility of microgrid systems.

Kim et al. [20] used HOMER in studying the feasibility of displacing a diesel generator (DG) as the only source of power for a tourist spot in the South China Sea, Malaysia. Results of their case study showed that a 20% reduction in NPC is available from solely using a DG versus having a Hybrid Renewable Energy System (HRES) composed of wind turbine (WT), solar photovoltaic (PV), converter (CONV) and back-up sources of power from DG and batteries (BT). Sen et al. [21] employed HOMER to meet the load demand coming from a residential, institutional, commercial, agricultural and small scale industry in India. The authors also presented post-HOMER analysis to discuss issues that might influence the realization of the optimal solution of their model.

HOMER has also been implemented to find the optimum sizing of a solar powered system to maintain water quality which impacts the fishery production system in Indonesia [22]. Additionally, Hafez and Bhattacharya [23] conducted four different studies using synthetic load generated from HOMER and resource data for Waterloo, Ontario, Canada. The study included diesel-only, a fully renewable-based, a diesel-renewable mixed, and an external grid-connected microgrid configuration. Montuouri et al. [24] dealt with the economic evaluation of a biomass gasification plant using HOMER while studying the integration of RE in microgrid coordinated with demand response resources. High profitability was demonstrated when using demand response to handle renewable variability. Lastly, Amutha and Rajini [25] examined growing energy demand among domestic, industrial, agricultural areas in a remote village in India through HOMER. The optimal options for RE based electrification were compared with the extended grid electricity distribution network for which the costs of extending lines to rural facilities were proven to be expensive.

A wide range of other modeling tools aside from HOMER, can be used in energy system design. There is already a large body of literature reviewing the features of various software-tools that can be used in simulating and optimizing an energy system. For example, interested readers are referred to the work of Tozzi and Jo [26], Ringkjøb et al. [27] and Connolly et al. [28] for broad and comprehensive analyses of various tools available to the energy modeling community.

Unlike the single objective function implemented in HOMER, Ming et al. [29] argued that the optimization of HRES should follow a multi-objective problem (MOP) approach for most cases. According to a study made by Konak et al. [30], MOP objectives are generally conflicting but they have to be considered simultaneously in describing complex engineering optimization problems. Thus, it is important to investigate a set of solutions versus a single solution (as is the case for conventional optimization techniques) while satisfying more than one objective function. Such solution diversity, as implemented through a multi-objective approach, is a research gap among recent energy studies done for the Arctic environment. This multi-objective approach of optimizing energy systems unlocks the full spectrum of solutions in the energy system design space.

Several examples of objective functions in solving MOP can be seen in Table 2. More detailed information of each objective can be found in the cited references; the specific objective functions used in this research work are further described in Sec. 2.1.1.

1.2. Research gap and study objectives

A research gap was identified in terms of addressing the complexity of designing energy systems for a unique environment like the Arctic. Decision makers study the Arctic from different viewpoints, thus, there exist multiple solution philosophies in exploring design alternatives that could work in Northern remote communities (to be discussed further in Sec. 2.1.1). Hence, the primary objective of this study is to extend the previous work of WWF by introducing a new modeling paradigm that can represent the complex trade-offs between priorities when designing an energy system for an Arctic community and remote communities in general. Since HOMER only considers NPC, it does not fully capture relevant aspects of the energy situation for Northern communities. This is also the case for WWF's in-house energy modeling tool, which is similarly based on NPC with an even simpler modeling treatment for its BT storage and a conventional dispatch strategy. Thus, the proposed method of this study aims to provide additional capabilities as compared to existing energy modeling platforms, and use the results to provide insights to policy makers in solving the *"trilemma"* of challenges relating to energy security, environmental emissions and energy economics.

Compared to previous and recent studies, the novelty of the present work is in developing a multi-objective optimization framework that captures complex trade-off in designing energy system for remote communities, while ensuring high power supply reliability with minimum impact to the environment and cost of living to the Indigenous peoples in the North. The tool is applicable beyond the bounds of the Canadian Arctic but its functionalities will be described through a case study while observing its relevance on an international perspective as well.

Relative to current energy trends and the research gap exposed in recent studies to capture trade-offs caused by the complexity of designing energy system within and beyond Arctic communities, the key contributions of this work can be summarized as:

1. Development of a multi-objective optimization framework that integrates complex trade-offs for Northern latitude community energy systems and other remote communities in general;
2. Robust simulation and optimization algorithms that can size components of a hybrid microgrid system while evaluating the impact of various operational strategies;
3. The baseline simulation results of the energy system model have been validated against widely accepted software HOMER;
4. A case study for Sachs Harbour, the Northernmost community in the NWT with extreme winter conditions has been completed, demonstrating applicability of the model to other Arctic and remote communities;
5. The utility of insights from a multi-objective algorithm have been demonstrated.

The rest of the article is organized as follows. Section 2 describes the models developed for the study and Section 2.4 presents information regarding the specific Arctic community that was studied. Section 3 summarizes the results, with conclusions and future work given in Section 4.

2. Methods

The schematic diagram of a prototypical hybrid energy system studied in this work is presented in Fig.3. It consists of WT, solar PV, BT storage and back-up power from a DG. A bi-directional converter was also modeled so power can flow in both directions (DC bus to AC bus and vice versa). Each distributed energy resource (wind, solar and various sources of power generation and energy storage) can be modeled individually. However, with the proposed Multi-objective INtegrated Energy System (MINES) model in this study, a system-of-systems approach was employed wherein the constituent systems were brought together in one integrated microgrid system as presented in Fig. 3 and Fig. 4.

2.1. Optimization module

A general constrained minimization problem may be written as follows:

$$\begin{aligned} \min_{x} \quad & f_s(x) && \text{s} = 1, 2, ..., S \\ \text{s.t.} \quad & h_p(x) = 0 && \text{p} = 1, 2, ..., P \\ & g_e(x) \leq 0 && \text{e} = 1, 2, ..., E \end{aligned} \tag{1}$$

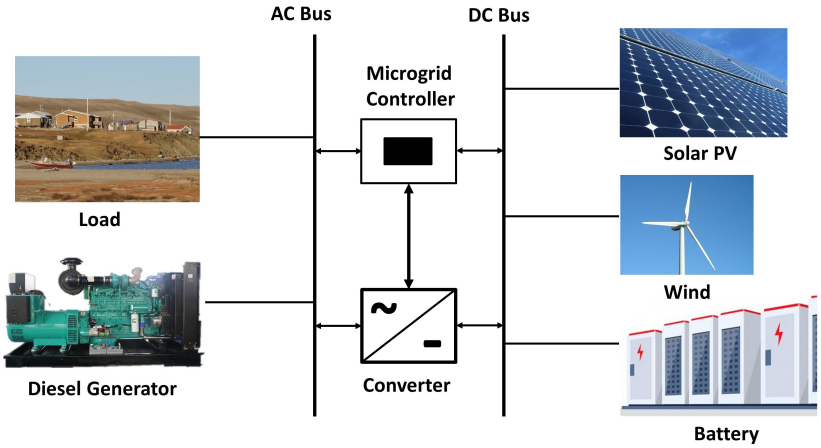

Figure 3: Schematic layout of a hybrid solar-wind-battery-diesel energy system.

where x is the decision vector (set of variables to be optimized); $f_s(x)$ is the objective function while $h_p(x)$ and $g_e(x)$ are the sets of equality and inequality constraints, respectively. The indices refer to the number of objective functions as well as the constraints of the model.

A genetic algorithm (GA) model has been developed to solve the optimization problem described in this study. It was first proposed by John Holland [40] and then widely utilized for optimization problems as popularized by Goldberg [41]. It is an optimization approach to determine the best outcome for a mathematical model following a certain set of constraints. Fig. 4 shows a flowchart of the GA as applied to modeling energy systems. It starts by inputting relevant information for the model such as load profile, meteorological data, equipment specifications and projected costs, among others; constraints were also added in the algorithm. The model generates initial set of individuals of a population randomly selected in each step of the algorithm which serve as basis for the next iteration [42]. The GA analyses random sizes of each component in the HRES while satisfying the load demand at each timestep. Each of the solutions in the population comprises a range of numbers called an individual, vector or chromosome [43]. After the first random configuration, the initial population set is evaluated based on the objective/fitness function defined in the model. This corresponds to minimizing costs, maximizing system reliability, and others. The three operators (selection, crossover, mutation) then come into play. The selection operator selects the predefined percentage of the initial population base on their fitness values [44]. The crossover operator generates new individuals by combining the information contained within a pair of parents with the goal of attaining higher fitness values. The process of looking for greater fitness values continues at each iteration and a mutation operator is needed to prevent the model getting stuck in a local minimum. Mahbub et al. [45] describes this concept as *"survival of the fittest"* ensuring that only the best individuals (solutions) have the chance to reproduce to the next generation. These new generations are produced in a loop until the termination criteria is met and the optimized solution is found.

Campana et al. [46] used GA as an optimization technique to find the best mix among power sources, storage systems and back-up sources of power while minimizing Life Cycle Cost (LCC) and maximizing power system reliability. Meanwhile, Konak et al. [30] provided an overview and tutorial of implementing a GA in an energy system model while describing its applicability in solving problems with multiple objectives. As well, Yang et al. [47] utilized a GA to optimally size a stand-alone hybrid solar-wind system with Loss of Power Supply Probability ($LPSP$) as their objective function. The decision variables included in their research were the number of solar PV modules, WT, slope angle of the PV array and the installation height of the WT. At the end of their case study, they found that a hybrid system with 3-5 days' battery nominal storage is suitable for the desired $LPSP$ of 1% and 2%.

For this study, the GA approach was implemented in a MATLAB® platform and the settings of the optimization parameters are listed in Table 3.

There are other optimization approaches that can be used in designing an energy system such as the classical optimization methods of linear programming or Mixed Integer Linear Programming (MILP). However, they are rarely used for multi-objective optimization functions and can only be

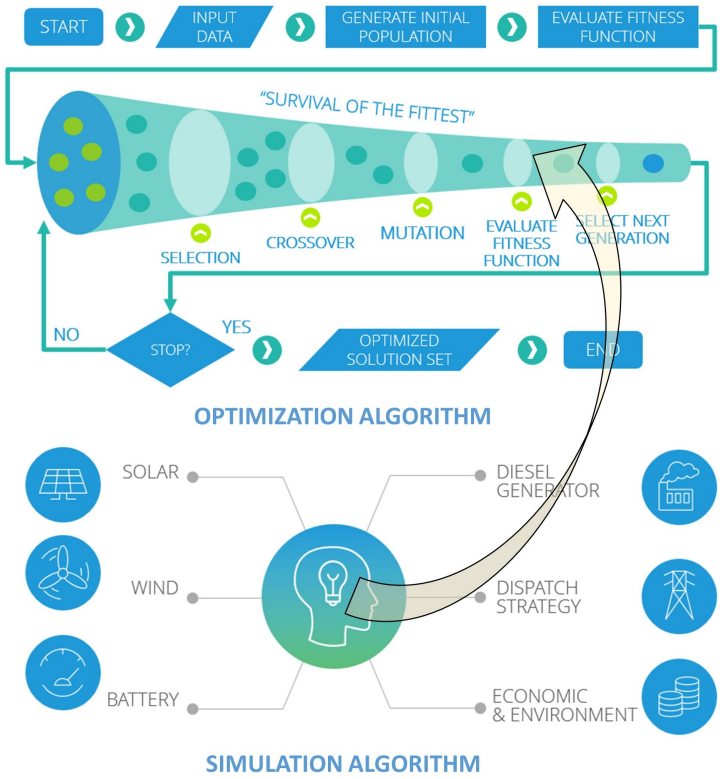

Figure 4: Flowchart of the optimization and simulation process.

applied to restricted types of problems due to non-linearities and other factors in real-world applications. Simplification of non-linear problems results in a lack of accuracy in the optimization process. In contrast, good performance for a wide range of different optimization problems is a significant advantage of GA [43]. It is commonly applied to solve different combinatorial optimization problems with a high number of feasible solutions that makes the application of MILP and other classical optimization methods challenging [49]. Further, non-linearities of different variables, multiple objective functions and constraints can be handled effectively by GA. Most importantly, GA requires information only from the objective/fitness function since the algorithm does not require derivatives which is the conventional way of finding minimum or maximum of a certain optimization problem; hence, it is able to deal with various non-linearities which are present in designing complex energy systems. Furthermore, the computational time is relatively low as compared to other optimization methods [50]. Interested readers are referred to the work of Tezer et al. [43] for evaluation of various multi-objective optimization approaches for sizing components of stand-alone HRES.

2.1.1. Objective functions, constraints and other output parameters

Based on the previous Energy Charrettes among the territories, affordability is a major concern for Indigenous peoples in the North [51]. Thus, the first objective in the optimization process is to minimize the Levelised Cost of Energy ($LCOE$). As compared to previous studies with NPC as the only objective function, $LCOE$ was necessary for this work to better understand the cost impact in terms of the actual electricity price being paid by the community versus the subsidy support from the government. The typical $LCOE$ equation [52] was modified in order to consider the full spectrum of costs from the design to recycling (salvage value) stage as shown in Eq. 2.

$$LCOE = \frac{\sum_{t=1}^{n} \frac{CC_i(t)+O\&M_i(t)+Z_i(t)-S_i}{(1+r)^t}}{\sum_{t=1}^{n} \frac{P_{gen}}{(1+r)^t}} \tag{2}$$

where t is time (year); r is the discount rate (%); n is the total life of the energy system (year); CC is the capital cost ($) per unit of the system's component i; $O\&M$ is the operations and

maintenance costs ($/year); Z is all other costs associated with the project ($/year); S is the salvage value ($); and P_{gen} is the power generated from the microgrid system (kWh/year).

The second objective is in line with Canada's goal to offset diesel [53] as the primary source of energy to remote communities. It was applied in the model by minimizing fuel consumption ($fuel_{cons}$) of the diesel generator. The mathematical equation involved is illustrated in Section 2.2.4 as part of the DG model.

The two objective functions arise from different stakeholders (community and policy makers) with varying solution philosophies to solve energy issues in the North. Power coming from the DG might be a cheaper option for the communities, but it degrades the Arctic environment. It might give energy security for remote areas but the risk of oil spills during fuel transport and storage will continue to be a concern for everyone living in the region. All of these competing factors can be effectively evaluated if they can be simultaneously considered and optimized in the model.

Various constraints were also implemented as part of the optimization algorithm. To consider energy security for example, $LPSP$ is set to 0%. An $LPSP$ of 100% means that the demand is never satisfied and an $LPSP$ of 0% means that the load is always satisfied. For instance, Nelson et al. [31] in their report, targeted an $LPSP$ of 0.0003 which corresponds to having a loss of power supply of approximately 1 day in 10 years. Other research work that implemented this technique can be found here [32, 54]. The mathematical expression of $LPSP$ over a given time period T (8760 h) can be written as:

$$LPSP = \frac{\sum_{t=1}^{T} P_{deficit}(t)}{\sum_{t=1}^{T} P_{load}(t)} \tag{3}$$

where $P_{deficit}$ pertains to the insufficient supply of power from the renewables and diesel, as well as the available energy from the BT storage:

$$P_{deficit}(t) = P_{load}(t) - (P_{RE}(t) + P_{DG}(t) + P_{batt}(t-1)) \tag{4}$$

where P_{load} is the electricity demand (kW);P_{RE} is the power produced by the renewables (kW); and P_{batt} is the power stored from the BT (kW).

The full set of constraints considered to run the optimization module of MINES are:

$$constraints \begin{cases} LPSP \leq 0\% \\ SOC_{min} \leq SOC(t) \leq SOC_{max} \\ RE_{pen} \geq 30\% \\ P_{excess} \leq 30\% \\ LCOE \leq 0.70 \frac{\$}{kWh} \\ DG_{LF} \geq 30\% \end{cases} \tag{5}$$

where SOC is the state of charge of the BT (%); RE_{pen} is the RE penetration (%); P_{excess} is the excess electricity (%); and DG_{LF} is the load factor of the DG (%). The 30% RE_{pen} target was based on the conservative assumption of including a portion of RE in the energy mix of the location being studied which is currently 100% diesel. The 30% P_{excess} was to avoid oversizing each component of the HRES. To establish a competitive price for the community as compared to their current price of electricity, an $LCOE$ limit of 0.70 CND $/kWh was imposed in the model, similar to the current price of Whati, NWT (Fig. 2(b)). The 30% DG_{LF} constraint was to avoid running the DG at partial load which is damaging for the generator and will be further discussed in Sec 3.1. The user can also change and add additional constraints in MINES or pick one objective function and formulate it as a constraint.

An example of an output parameter that can also be extracted from the model relates to the life cycle emissions of the system. Emission factors from Roberts et al. [55] were adapted for this study and it is shown in Table 4. As compared to considering the emissions from fuel only, a life cycle approach covers both direct and indirect emissions generated during the manufacturing, transportation and decommissioning stages from all components of the microgrid system.

In addition to $LCOE$, another economic performance metric was introduced in Table 11. The metric was parameterized as Life Cycle Cost (LCC) of the energy system. It served as one of the simulation outputs of the model to complement $LCOE$ and to capture the full cost of the system

throughout its entire life cycle [43]. It is also the numerator of the modified $LCOE$ equation in Eq. 2.

2.1.2. Design optimization variables

The decision variables used for this research are divided into three groups. The first group of variables pertains to the individual capacity of all components of the HRES in Fig. 3 (solar PV, WT, BT, DG and CONV). The second group relates to the quantity of each component as listed in Table 5. The third group refers to the operation dispatch strategies of the integrated microgrid system. In total, there were 11 discrete decision variables carried out in the model.

2.2. Simulation module

The simulation module is part of the overall energy system model. Simulation results were evaluated per generation in MINES, in the form of fitness function on a one hour timescale over a year (Fig. 4). Community-scale models usually employ 1-hour temporal resolution on a one-year timeframe to size and investigate components of the energy system. Regional-scale models, on the other hand, use low temporal resolution (every 5 years or per decade) to capture a broader space in their study. One-hour temporal scale on a yearly basis is a common academic practice [56, 55] in sizing components of the microgrid system of a specific community. Increasing the temporal resolution of the model will be too computationally expensive for the model to converge to a solution in a design relevant timeframe. For this reason, sensitivity analysis is implemented in this work in order to address uncertainties and to test the robustness of the results of the model.

The mathematical models of each subcomponent of the microgrid system will be discussed in the following subsections.

2.2.1. Solar Photovoltaic model

The amount of solar PV output is based on the resource potential of a given location which is parameterized by the Global Horizontal Irradiance (GHI). It pertains to the intensity of solar radiation striking the horizontal surface of the earth. This parameter has been translated to its corresponding radiation incident on the surface of the PV array (POA) by quantifying POA's three radiation components, namely beam radiation, reflected radiation, and diffuse radiation. Methods proposed by Duffie and Beckman [57] as well as Erbs et al. [58] were used at this point of the PV model. After identifying POA, the mathematical experession to quanitfy PV generation is then expressed as follows [59]:

$$P_{pv} = Y_{pv}\left(\frac{POA}{POA_{STC}}\right)[1 + \alpha_p(T_c - T_{c,STC})]f_{PV} \tag{6}$$

where P_{pv} is the power delivered by the PV array (kW); Y_{pv} is the rated capacity of the PV array (kW); POA_{STC} is the incident radiation at standard test conditions (STC) (1 kW/m^2); α_p is the temperature coefficient of power (%/°C); T_c is the PV cell temperature in the current timestep (°C); $T_{c,STC}$ is the PV cell temperature under STC (25 °C); and f_{pv} is the derating factor (%) which accounts for reduced PV output in real-world operating conditions.

The PV cell temperature (T_c) per timestep as described in Eq. 6 was accounted using the approach given in Eq. 7 [59].

$$T_c = \frac{T_a + (T_{c,NOCT} - T_{a,NOCT})\left(\frac{POA}{POA_{NOCT}}\right)\left[1 - \frac{\eta_{mp,STC}(1 - \alpha_p T_{c,STC})}{\tau\alpha}\right]}{1 + (T_{c,NOCT} - T_{a,NOCT})\left(\frac{POA}{POA_{NOCT}}\right)\left(\frac{\alpha_p \eta_{mp,STC}}{\tau\alpha}\right)} \tag{7}$$

where T_a is the ambient temperature (°C); $T_{c,NOCT}$ is the nominal operating cell temperature (NOCT) (°C); $T_{a,NOCT}$ is the ambient temperature at which NOCTis defined (20 °C); POA_{NOCT} is the solar radiation at which NOCT is defined (0.8 kW/m^2); $\eta_{mp,STC}$ is the maximum power point efficiency of PV under STC (%); and $\tau\alpha$ is the effective transmittance-absorptance product of the PV module valued at 0.9 according to Duffie and Beckman [57]. The PV parameters used in the simualtion are shown in Table 6.

2.2.2. Wind turbine model

Jain [60] and Burton et al. [61] defined basic to complex concepts of modeling wind as applied to an energy system. The most fundamental approach to correlate wind speed and wind power is:

$$P_w(t) = \frac{1}{2}\rho_a A C_p u(t)^3 \eta_{gen} \tag{8}$$

where P_w is the output power of the WT (kW); ρ_a is the air density (kg/m^3), A is the rotor area (m^2); C_p is the power coefficient (%); u is the wind speed (m/s) at time t; and η_{gen} is the efficiency of the generator (%).

The extractable power output of the wind resource is influenced by the hub height of the turbine. In general, as hub height increases, wind speed increases as well (known as wind shear). The magnitude of wind shear differs per site and is dependent on factors like wind direction, wind speed and atmospheric stability. By determining wind shear, the modeler can extrapolate the wind speed or wind-power-density to other heights by using the following equations:

$$\begin{aligned} P_w(h) &= P_w(h_a)\left(\frac{h}{h_a}\right)^{3\alpha} \\ u(h) &= u(h_a)\left(\frac{h}{h_a}\right)^{\alpha} \end{aligned} \tag{9}$$

where $P_w(h)$ and $P_w(h_a)$ are power generated (kW) at hub height h (m) and anemometer height h_a (m), respectively, and α is the power law exponent (•); same analogy applies in terms of wind speed u (m/s).

Wind speed is a stochastic quantity. Thus, to model wind speeds, a statistical distribution, typically a Weibull distribution for hourly wind speed is needed. The distribution follows the function [61] given in Eq. 10.

$$F(u) = exp\left(\left(-\frac{u}{c}\right)^k\right) \tag{10}$$

where $F(u)$ describes the percent of time hourly mean speed exceeds u (%); c is a scale parameter (•); and k pertains to the variability about the mean (•). The relation of annual mean wind speed $\bar{U}$ and c is in Eq. 11.

$$\bar{U} = c\Gamma\left(1 + \frac{1}{k}\right) \tag{11}$$

where Γ is the complete gamma function (•).

Further to the theoretical extractable wind power in Eq. 8, the WT model for this study incorporated actual power curves from the turbine manufacturers and wind power was approximated using the piecewise interpolation function in Eq 12 [62].

$$P_w(u) = \begin{cases} P_{w,r}\frac{u^2 - u_{ci}^2}{u_r^2 - u_{ci}^2} & \text{if } u_{ci} < u < u_r, \\ P_{w,r} & \text{if } u_r < u < u_{co}, \\ 0 & \text{if } otherwise. \end{cases} \tag{12}$$

where $P_{w,r}$ is the rated power output of the WT (kW); u_{ci} is the cut-in wind speed or the speed where the turbine starts producing energy (m/s); u_{co} is the cut-out wind speed or the speed where the turbine stops operating (m/s); and u_r is the rated wind speed on which the rated power of the turbine is produced.

The wind turbine specifications used in the simulation are shown in Table 7 and their corresponding power curves are presented Fig. 5. The manufacturers of the chosen wind turbine types have extensive track records in Northern Canada and Alaska. The turbines have been proven to operate even in cold climate conditions. Finally, the actual power generated by the WT was calibrated by considering the variation of air density with a method adapted from [55].

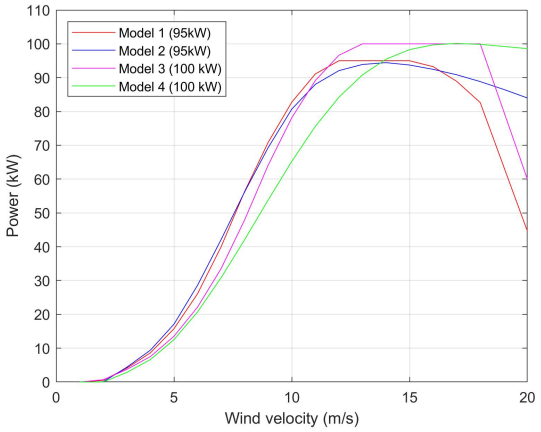

Figure 5: Power curves of the wind turbines used in the simulation.

2.2.3. Kinetic battery storage model

The energy storage model used for the study follows the Kinetic Battery Model (KiBaM) of Manwell and McGowan [63]. It is a two-tank model based on the approach of chemical kinetics. It assumes that the charge can be stored in two ways – either as immediately available or as chemically bound.

KiBaM requires determination of three parameters in order to describe the behavior of the lead acid BT: q_{max} is the maximum capacity of the BT (Ah); c_{BT} is the fraction of capacity that may hold available charge of the BT (•); and k_{BT} is the rate constant of the BT (•). Considering the nominal system voltage, the mentioned parameters were used in quantifying the respective maximum BT charge power (given $I_{c,max}$ in Eq. 13) and maximum BT discharge power (given $I_{d,max}$ in Eq. 14) per timestep.

$$I_{d,max} = \frac{-k_{BT}c_{BT}q_{max} + k_{BT}q_{1,0}e^{-k_{BT}\Delta t} + q_0 k_{BT}c_{BT}(1-e^{-k_{BT}\Delta t})}{1 - e^{-k_{BT}\Delta t} + c(k_{BT}\Delta t - 1 + e^{-k_{BT}\Delta t})} \tag{13}$$

$$I_{c,max} = \frac{k_{BT}q_{1,0}e^{-k_{BT}\Delta t} + q_0 k_{BT}c_{BT}(1-e^{-k_{BT}\Delta t})}{1 - e^{-k_{BT}\Delta t} + c(k_{BT}\Delta t - 1 + e^{-k_{BT}\Delta t})} \tag{14}$$

where $q_{1,0}$ is the available charge at the beginning of the timestep (Ah) and q_0 is the stored energy. Meanwhile, the resulting available (q_1) and bound (q_2) charges at the end of every timestep were approximated by the succeeding equations.

$$q_1 = q_{1,0}e^{-k_{BT}\Delta t} + \frac{(q_0 k_{BT}c_{BT} - I)(1-e^{-k_{BT}\Delta t})(Ic_{BT}(k_{BT}\Delta t - 1 + e^{-k_{BT}\Delta t})}{k_{BT}} \tag{15}$$

$$q_2 = q_{2,0}e^{-k_{BT}\Delta t} + \frac{q_0(1-c_{BT})(1-e^{-k_{BT}\Delta t}) - I(1-cBT)(k_{BT}\Delta t - 1 + e^{-k_{BT}\Delta t})}{k_{BT}} \tag{16}$$

$$q_0 = q_{1,0} + q_{2,0} \tag{17}$$

where $q_{2,0}$ is the bound charge at the beginning of the timestep (Ah).

The model assumes the convention that the power surplus from the renewables will cause negative current indicating that the BT is charging and the power deficit will translate to a positive current leading to discharge of power from the BT. The simulation adapts the BT degradation (R_{BT}) model of HOMER. Mathematically, storage degradation is determined using the following equation with both use and aging components:

$$R_{BT} = \begin{cases} \frac{N_{BT}Q_{LT}}{Q_{thrpt}} & \text{if } limited\,by\,throughput, \\ R_{BT,f} & \text{if } limited\,by\,time, \\ min\left(\frac{N_{BT}Q_{LT}}{Q_{thrpt}}, R_{BT,f}\right) & \text{if } limited\,by\,both. \end{cases} \tag{18}$$

where N_{BT} is the number of BT in the storage bank (•); Q_{LT} is the lifetime throughput of a single storage (kWh); Q_{thrpt} is the annual storage throughput (kWh/yr); and $R_{BT,f}$ is the storage float life (years).

The storage specifications used in the simulation model are listed in Table 8.

2.2.4. Diesel generator model

In various models [64, 65], a linear relationship is assumed between fuel consumption ($fuel_{cons}$) and the corresponding DG output. Mathematically, it is defined as:

$$fuel_{cons} = F_0 P_{DG,r} + F_1 P_{DG} \tag{19}$$

where F_0 is the fuel curve intercept coefficient (L/h/kW$_{\text{rated}}$); F_1 is the fuel curve slope coefficient (L/h/kW); $P_{DG,r}$ is the rated capacity of DG; and P_{DG} is the instantaneous power coming from the DG (kW).

The simulation parameters for the generator are presented in Table 9.

2.3. Operation strategies

Two operation strategies were implemented in the model: Load following (LFOS) and Cycle charging (CCOS). For both strategies, the generator only operates when the renewables cannot meet the load and the BT cannot discharge power. However, when the dispatch is in LFOS mode (Fig. 6), the generator produces just enough power to meet the instantaneous load per timestep unless it reaches the minimum power of the DG based on DG_{LF}. In CCOS, on the other hand, the DG runs at full rated capacity (Fig. 7) and will continue to operate and charge the BT up to a pre-set SOC (SOC_{sp}). Regardless of the operational strategy, any excess electricity production was assumed to be dispatched to a dummy load.

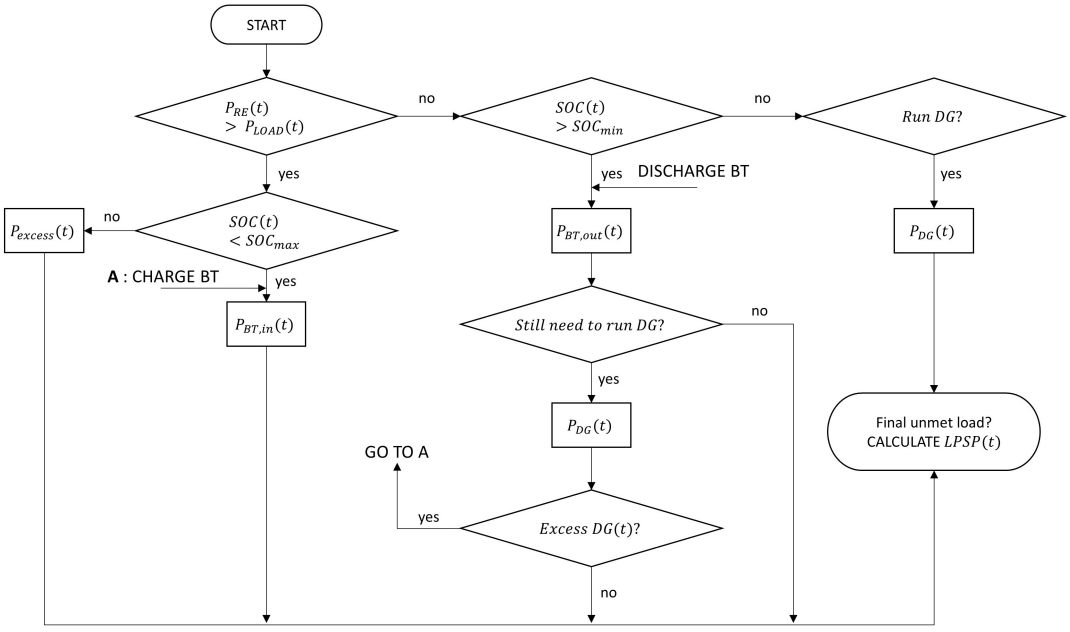

Figure 6: Flowchart of load following operation strategy.

Finally, to manage power flows from the DC bus to AC bus and vice versa, the simulation parameters for the converter listed in Table 10 were used.

2.4. Case study input data

The proposed method was applied to the Northernmost community in NWT: Sachs Harbour (Lat: 71.9884 N; Long: 125.23935 W). The community is located on Banks Island in the High Arctic as presented in Fig. 8. It has a population of about 130 and it is the ancestral territory of the Inuvialuit [66]. The community's main source of electrical power is diesel with a total generating capacity of 795 kW. The diesel generation facility is owned and operated by the Northwest

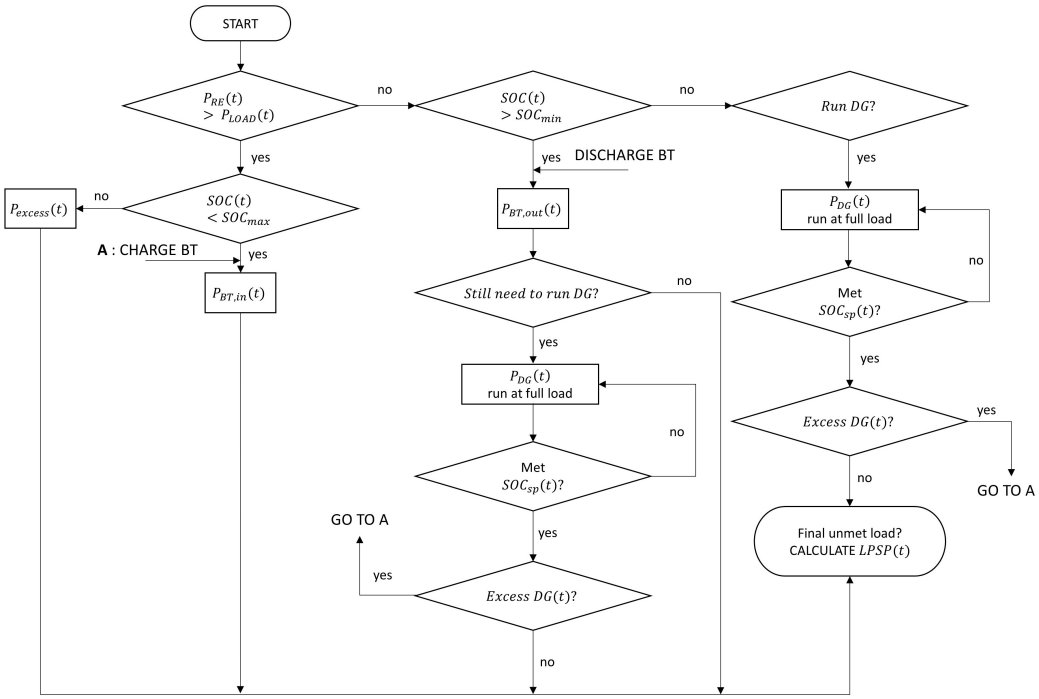

Figure 7: Flowchart of cycle charging operation strategy.

Territories Power Corporation (NTPC). The fuel is shipped by Marine Transportation Services by barge once a year through NTPC's fuel service division. Since year-round road access to the community is not available, fuel is shipped via plane if the barge is unable to deliver the community's fuel.

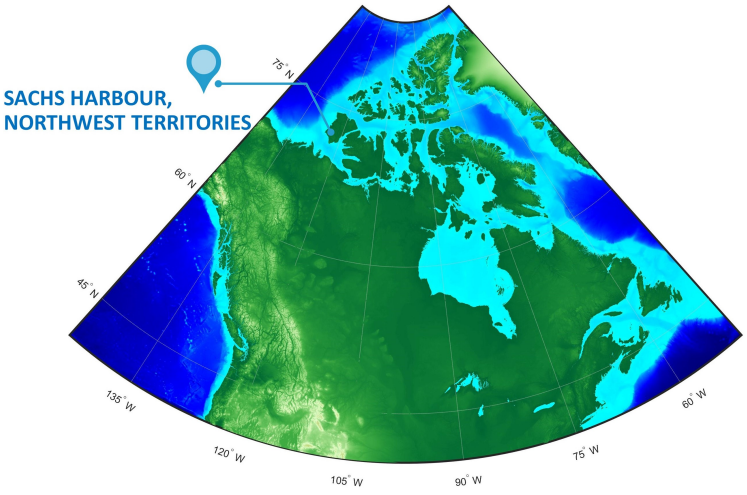

Figure 8: Geographical location of Sachs Harbour in reference to rest of Canada.

Fig. 9(a) shows the hourly load profile of Sachs Harbour. The actual load data came from NTPC with a 15-minute temporal resolution for one year. The maximum and minimum loads are 220 kW and 70 kW, respectively. The average daily consumption profile for the different seasons is also shown in Fig. 9(b).

Actual wind tower measurements with a 10-minute temporal resolution were extracted from July 8, 2005 to September 29, 2009; data was requested for this study from the GNWT office. The data was initially used for the wind energy feasibility project done by GNWT. The wind meteorological instruments were located 6.5 km west of the Sachs Harbour airport along the main road. It was equipped with three anemometers and one wind vane at three measurement heights as presented in Fig. 10(a). The variations of the wind velocity every 10 minute at 30m height is

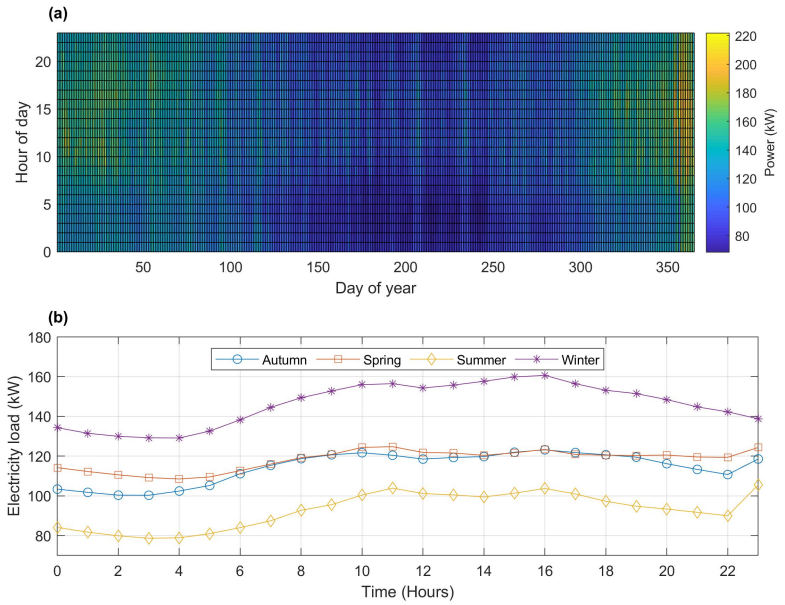

Figure 9: Electricity load consumption of Sachs Harbour: (a) Average hourly load profile for one year; (b) Average hourly load profile for the different seasons.

also shown in Fig. 10(b). All anemometers used were NRG 40 model and the wind vane was a NRG 200P model. Fig. 11 shows that the dominant wind direction of the community is blowing from the southeast.

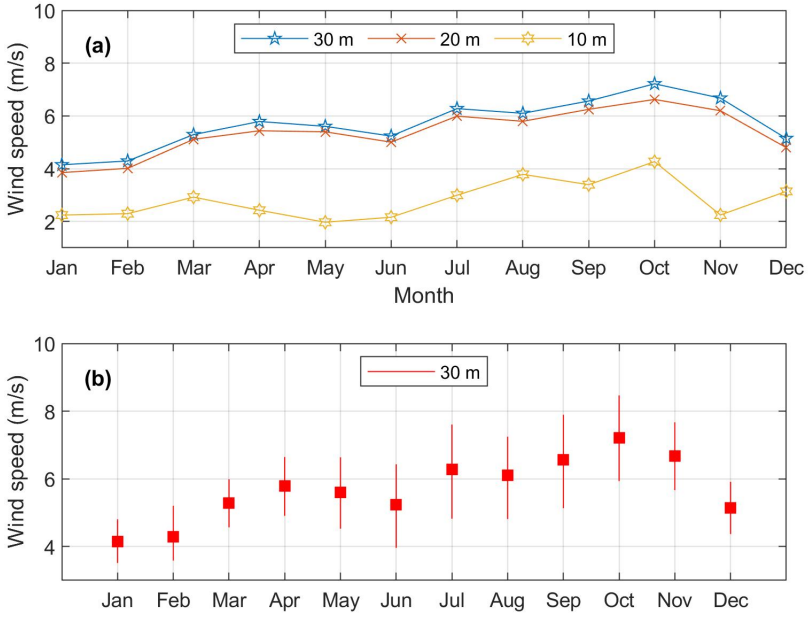

Figure 10: Wind speed profile of Sachs Harbour from July 8, 2005 to Sept 29, 2009: (a) Average monthly wind speed at three measurement heights; (b) Average monthly wind variations of wind speed recorded for every 10 minutes.

Actual wind shear was calculated from the three respective wind measurement heights and wind velocity was extrapolated at a 40m height according to the method discussed in Sec 2.2.2. The resulting wind profile after the extrapolation is presented in Fig. 12, with its corresponding histogram and Weibull fit distribution shown in Fig. 13. High wind speed registries can be observed during autumn and the mean wind velocity for the year is around 8m/s at a 40m height.

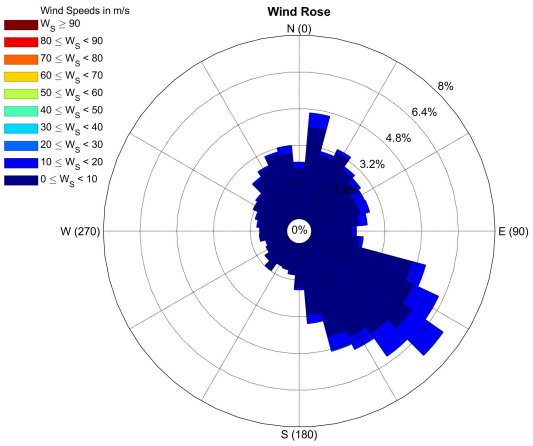

Figure 11: Wind rose profile of Sachs Harbour.

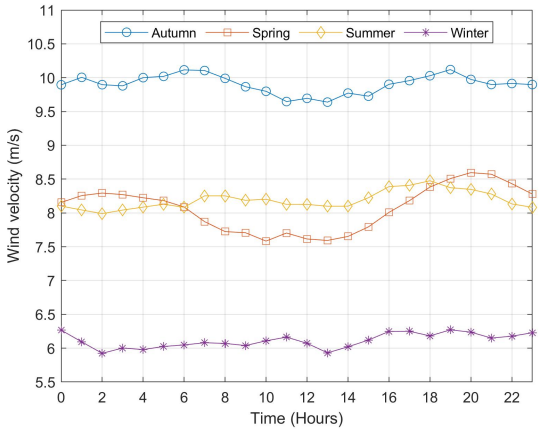

Figure 12: Average extrapolated wind speed of Sachs Harbour at 40m elevation for different seasons.

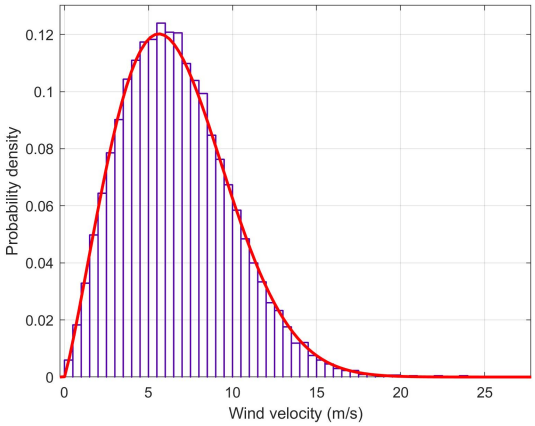

Figure 13: Histogram (violet bar) and Weibull fit distribution (red curve) of the extrapolated wind speed data at 40m elevation.

Other meteorological variables such as GHI and the community's temperature profile are shown in Fig. 14(a) and Fig. 14(b), respectively. The solar resource is low during autumn and winter due to extreme freezing temperature conditions. The data for GHI was extracted from GNWT's HOMER simulation file while the temperature timeseries data was retrieved from Meteonorm [67].

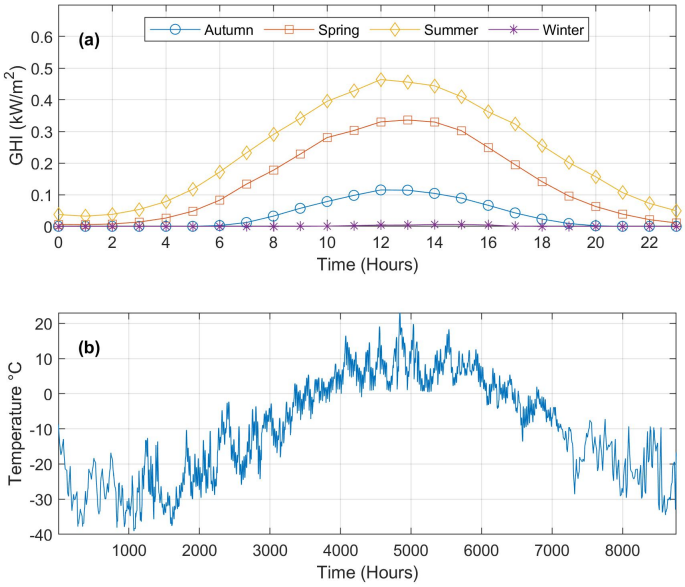

Figure 14: Other meteorological variables in Sachs Harbour: (a) Average hourly Global Horizontal Irradiance; (b) Hourly temperature profile for one year.

3. Results and discussion

This section presents the simulation and optimization results using the input data discussed in Sec. 2.4. The impact of the two operation strategies on the overall microgrid system was explored and sensitivity analysis was performed to investigate multiple system configurations that can be viable for Sachs Harbour. The robustness of the results was tested by modeling system component failure of each component of the hybrid system. Policy insights were framed considering various quantitative outputs extracted from MINES. At the end of this section, the results from the model were verified using an industry and academic accepted energy modeling tool, HOMER.

3.1. Optimization and simulation results

The optimized configurations of the energy system are shown in the form of a Pareto front in Fig. 15. The number of generations and population used to run the GA model is 200 and 100, respectively. Population size specifies the number of individuals in each generation. With a large population size, the GA analyses the solution space more thoroughly, thereby, reducing the chance that the algorithm is stuck in a local minimum versus the desired global minimum. However, a large population size also causes GA to run more slowly. As presented in Fig. 16, a wide range of values for the objective functions can be seen at the beginning of the optimization process but start to converge to a solution roughly at the 90th generation moving forward. This shows that MINES can no longer improve the $LCOE$ and $fuel_{cons}$; thus, the solution has been attained. The total number of possible combinations given the constraints in Eq. 5 and the dimensions of optimization variables listed in Table 5 is 2.8613 x 10^{14}. The algorithm converged to a solution in roughly 3h using a Windows 10 computer equipped with a 64-bit operating system, an Intel Core i7-7700HQ 2.800GHz and 16 GB of RAM.

Solutions of interest from the Pareto front are highlighted in Fig. 15 and listed in Table 11. It can be observed that lowering $fuel_{cons}$ resulted in an increase in $LCOE$ which was attributable to limiting the operation of the DG and replacing it with RE technologies. The uppermost left red marker in Fig. 15 represents the solution with lowest $LCOE$ and highest $fuel_{cons}$. On the other hand, the lowest right red marker corresponds to a solution with the highest $LCOE$ and lowest $fuel_{cons}$. The red marker at the middle of the curve is considered a trade-off solution for both $LCOE$ and $fuel_{cons}$. The discontinuities in the Pareto front were caused by the discrete characteristics of the optimization variables (as discussed in Sec 2.1.2) and the restrictions imposed in the constraints of the optimization algorithm which were mainly to limit the vast search space of solutions.

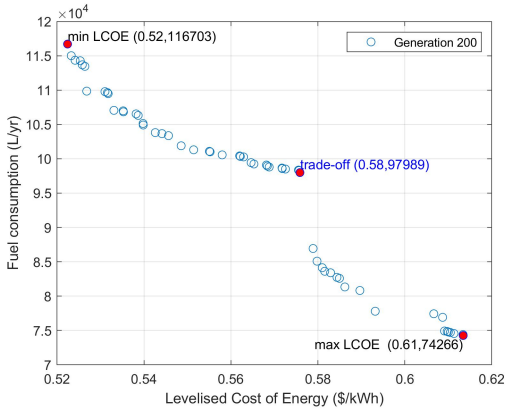

Figure 15: Pareto front of the last generation and the identified solutions of interest.

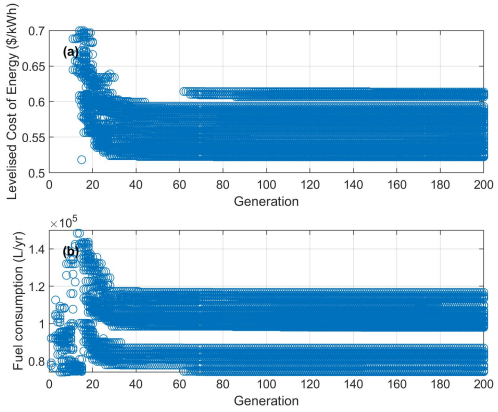

Figure 16: Variations of the objective functions during the multi-objective optimization process: (a) Levelised Cost of Energy objective function; (b) Fuel consumption objective function.

The power generated by the WT is the highest among all other sources of energy in the system for the three solutions. This reflects strong wind resource in the region and a viable option specifically for Sachs Harbour. Due to extended winter conditions in the Arctic, the share of solar PV is minimal and unmet load has to be met by either DG or discharging the power coming from the BT. The variations of *SOC* for the three solutions is presented in Fig. 17. The *SOC* profile of each BT was influenced by the operational dispatch strategy of the system as discussed in Sec. 2.3. The flows of electricity from the DC and AC bus were also constrained by the selected 250 kW CONV of the system which is the same for all three cases.

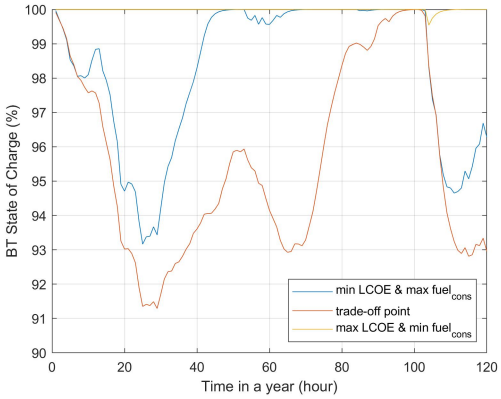

Figure 17: Performance variations of the state of charge of the BT for the three solutions of interest.

As listed in Table 11, the algorithm selected CCOS as the most appropriate operation strategy

for the three solutions. This shows that operating the DG uninterrupted in low power load mode can lead to higher fuel consumption resulting in higher oil residue in the engine as well. The residue has a negative impact on the functional behaviour of the engine and it decreases the expected lifespan of the generator. As a result, operations and maintenance costs of the DG increase whenever it is being partially utilized.

The effect of modifying the operation strategies was evaluated by changing the power dispatch and running the model once again. In Fig. 18, it can be noticed how the Pareto front moved right after constraining the operation strategy to LFOS. From this behaviour, it can be inferred that the CCOS is a better option economically for the microgrid system. In other words, running the DG at full rated capacity is more favorable than running it based on the unmet load per timestep. In addition, the engine cools down when running the generator in low load mode. As a result, the fuel is partially burned which produces relatively higher hydrocarbon emissions as compared to running it at full load.

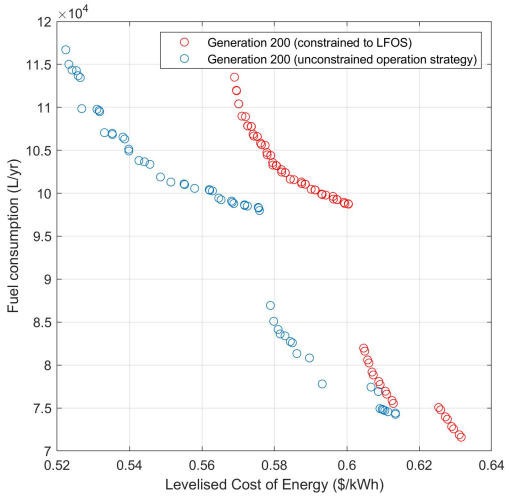

Figure 18: Plot showing how the Pareto front moved away from the unconstrained operation strategy to being limited to load following dispatch of power.

The energy mix of the system both hourly and monthly is presented in Fig. 19. For example, in a given year, it is possible that some of the load will be met only by WT or DG. Hence, for presentation purposes, a portion of the simulation results were selected where all available power sources were represented to show the actual variation of dispatch of power hour by hour. As expected, power output coming from the DG was higher during CCOS than LFOS (Fig. 19(a) and Fig. 19(b)) since the former was running at full load capacity until the pre-set SOC_{sp} of 80% was attained. The latter, on the other hand, dispatches exact power from DG based on the load not served by the renewables and BT. However, it can be observed that regardless of the operation strategy (Fig. 19(c) and Fig. 19(d)), wind has a significant share in meeting the load demand of Sachs Harbour.

The pre-set SOC_{sp} of 80% is an input parameter in the model which is only applicable when the system runs at CCOS. The value was set to 80% in order to prevent the BT from spending at a low SOC level which helps the storage bank from being damaged. Further, this will reduce the number of times the DG starts (since it is always running at full load) and it will also limit the number of charge-discharge cycles of the BT .

3.2. Design space sensitivity analysis

A sensitivity analysis was conducted by investigating other feasible energy system configurations for Sachs Harbour given the same optimization variables and restrictions implemented earlier in the study. Fig. 20 shows the location of each scenario in the Pareto space. Due to the currently available DG facility in the community and to seek realistic results, all configurations included DG and it was treated as a back-up source of power for the community along with the BT . Scenarios such as PV-DG, WT-DG and PV-WT-DG resulted in only one solution point on the Pareto front. As expected, a BT is required for RE integration. Multiple points, on the other

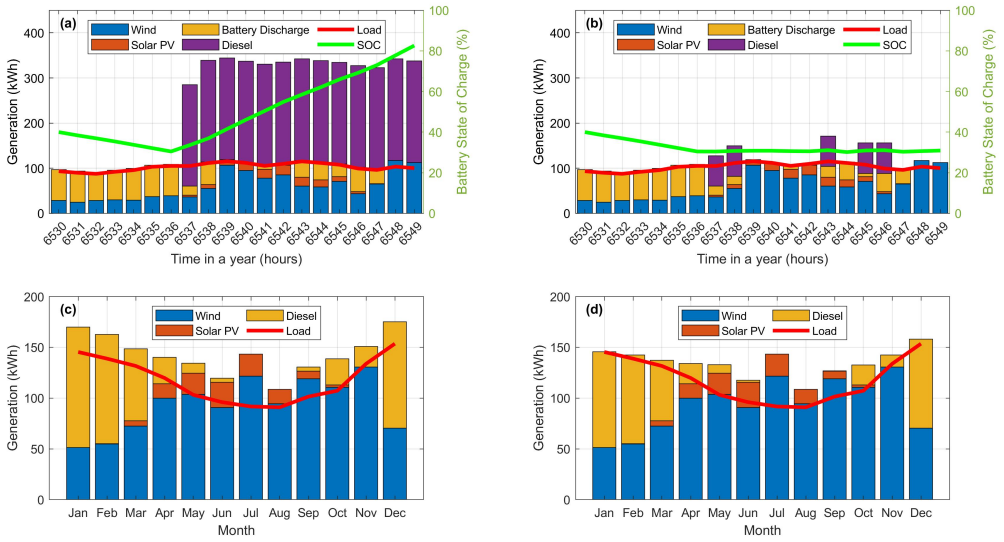

Figure 19: The solution with minimum LCOE and maximum fuel consumption was modified in terms of operation strategy to see the effect on the simulation results: (a) Hourly simulation results under Cycle Charging strategy; (b) Hourly simulation results under Load Following strategy; (c) Average monthly simulation results under Cycle Charging strategy; (d) Average monthly simulation results under Load Following strategy.

hand, were determined to be feasible after running the optimization algorithm for PV-BT-DG and WT-BT-DG. The Pareto front of the original system configuration (PV-WT-BT-DG) was retained in order to compare other feasible cases. Configurations with multiple solution points in the Pareto space reflect more flexibility for the community in their decision making process relative to sizing and designing each component of the energy system. The GA failed to find a feasible solution using DG as the only available source of power because of the restrictions given in the constraints and the goal of minimizing $fuel_{cons}$.

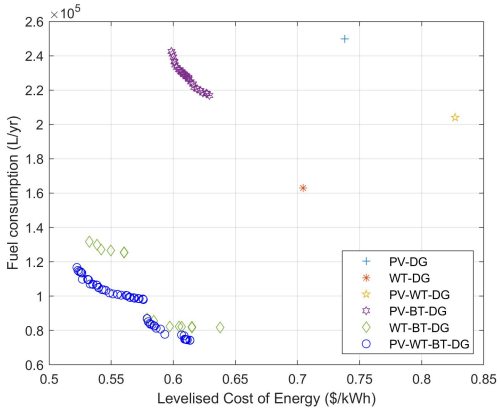

Figure 20: Pareto front of different scenario configurations.

Fig. 21 shows the annual generation of each scenario configuration and its corresponding emission reduction. Other performance metrics for each case are presented in Table 12 based on the lowest $LCOE$ of all possible combinations of various components of the hybrid microgrid system. For all scenarios, an $LPSP$ of 0% was imposed on the model to ensure load was met by either renewables, BT or DG; their optimal capacities are influenced by the range of the optimization variables in Table 5. Increasing the range of those variables translates to a wider search space and can add more time before the algorithm converges to a solution. For comparison with other scenarios, it was also assumed that a business-as-usual (BAU) case of DG with a capacity of 300

kW[4] was simulated in the model. Table 12 shows that the PV-WT-BT-DG hybrid system is the most suited energy system in the community of Sachs Harbour considering lowest values of its $LCOE$ and LCC. The proposed system has a significant amount of diesel fuel saved amounting to 353,407 L/yr in reference to the BAU scenario.

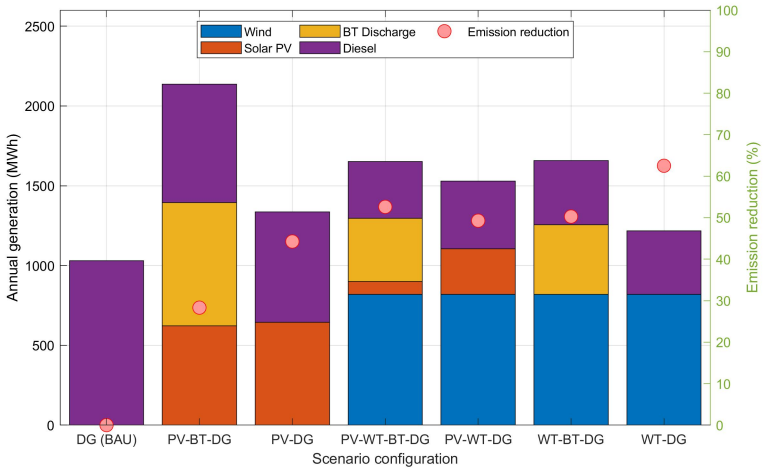

Figure 21: Annual power generation and projected emission reduction based on the lowest LCOE of each Pareto front of various system configuration.

3.3. Optimal system complexity

As the optimal system is complex with all types of components present, analysis of system component failure based on the PV-WT-BT-DG hybrid system configuration was also simulated in MINES. This section also highlights the robustness of the optimal results against uncertainties caused by the renewables in the hybrid system.

Fig. 22 shows the resulting system's $LCOE$ and $fuel_{cons}$ if one component fails and the system has to continue operation to meet the demand. This reflects challenges with seasonal repair in the North. It was observed that the DG was critical to the overall performance of the microgrid, resulting in 27% $LPSP$ assuming it failed. Failure of all other system components (PV or WT or BT or CONV), on the other hand, would not affect the security of power supply ($LPSP = 0\%$) but resulted in an increase in P_{DG} and $fuel_{cons}$ to compensate for the unavailability of a system component as shown in Table 13. Due to the significant share of power produced by the two WT and assuming it both failed during system operation, the $fuel_{cons}$ would increase by 228% (382,895 L/yr) as compared to a no-failure-scenario of the hybrid system. Similarly, a failure of the microgrid's CONV would force all the renewables and the BT storage to shut down, requiring the DG to operate as the community's only source of power; this case has an estimated 255% increase (414,280 L/yr) of $fuel_{cons}$. Failure of the BT in the system resulted in 71% increase in $fuel_{cons}$ due to the unavailability of a storage device to store surplus power (to be discharged if there is power deficit in the system) forcing the DG to run more often. Due to the PV's minimal share in meeting the demand, the estimated increase in $fuel_{cons}$ if it fails is only 13% (132,028 L/yr).

Assuming all the components of the hybrid system are the same and one WT is in operation, the model estimated a 41% decrease in $fuel_{cons}$ from the 382,895 L/yr mentioned earlier. Meanwhile, $fuel_{cons}$ is almost the same after doubling or increasing the capacity of the BT storage along with one WT operating, due to the microgrid's designed power dispatch (CCOS). Under this scheme, the DG operates until the SOC_{sp} of 80% is attained. In effect, the majority of the power deficit from the renewables was met by the DG instead of discharging the BT. The 220 kW peak load of Sachs Harbour and the 225 kW optimized capacity of the DG also affected this result.

[4]Sachs Harbour has a total generating capacity of 795 kW composed of three DG units with a capacity of 175 kW, 300 kW and 320 kW respectively. However, the generators are old (43-year-old plant) and they mostly run below 200 kW.

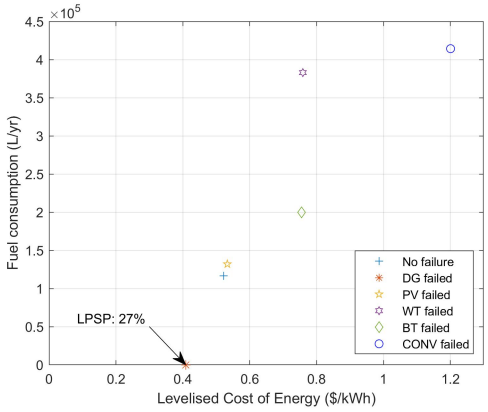

Figure 22: System component failure simulation of the fully hybrid (PV-WT-BT-DG) microgrid system.

3.4. Policy implications

Huntington et al. [68] argued that the purpose of energy modeling is to produce insights and not just numbers. Hence, this section provides policy insights that can be extracted from the analytical outputs of MINES. The proposed model can guide decision makers in transitioning Northern communities of Canada to more sustainable sources of energy. Similarly, given specific inputs, the quantitative model outputs from the tool can be applicable as well even beyond the bounds of the Canadian Arctic.

As discussed earlier, MINES generates sets of feasible solutions, in the form of a Pareto front, by analyzing possible combinations of various energy resources including the BT storage. For example, as of writing, Sachs Harbour has been awarded 10M CND from the federal and territorial governments to replace its 43-year-old diesel facility by 2020 [69]. With MINES, the policy makers can be informed of the investment pathways in upgrading diesel facilities from other Northern communities or spending its money to advance RE projects in the Canadian Arctic region. With the multi-objective nature of the model, policy makers can weigh different priorities and targets (energy security, affordability, environmental impact) which vary per community in the North. Specifically, the Pareto front can give insights to the decision making process of policy makers in giving preference to certain solution over the other by analyzing trade-off points and its corresponding pros and cons.

Fig. 23 shows the projected savings in subsidizing fuel cost as compared to DG (BAU) and the proposed hybrid system (PV-WT-BT-DG). The full cost of energy using the DG to meet the demand is 111 CND cents/kWh which is comparable to the price of Kugaaruk, Nunavut in Fig 2(b). The full cost of energy for the hybrid system, on the other hand, is 52 CND cents/kWh as listed in Table 12. The green bar in Fig. 23 pertains to the actual electricity price charged to the consumers of Sachs Harbour which is at 28 CND cents/kWh. The orange bar represents the subsidy price covered by the government to pay the full cost of producing electricity. Assuming full implementation of the proposed hybrid system, the government can save 70% from its budget in subsidizing the electricity cost of the community. The savings can then be allocated in increasing RE investments in Sachs Harbour or other areas in the NWT. The savings were calculated in reference to the actual subsidy paid by the government instead of savings per household in order to avoid uncertainty caused by disaggregating the community load data.

Another policy application of the model is in terms of the carbon pricing scheme in the Canadian territories [70]. As a signatory to the Pan-Canadian Framework for Clean Growth and Climate Change, GNWT committed to meeting a federal benchmark for carbon price by 2019. With this context, MINES can also be a tool in updating NWT's carbon price in the future to increase the penetration of RE while ensuring minimum impact on the cost of living in the Northern communities. This can be achieved by analyzing trade-offs between environmental emissions, cost of energy, energy security and other parameters that can be quantitatively analyzed by MINES.

3.5. Validation

The results of the model were validated using an industry and academic accepted energy modeling tool, HOMER. Since the presented multi-objective model and the full factorial optimization approach of HOMER are uncomparable, the simulation results were analyzed instead.

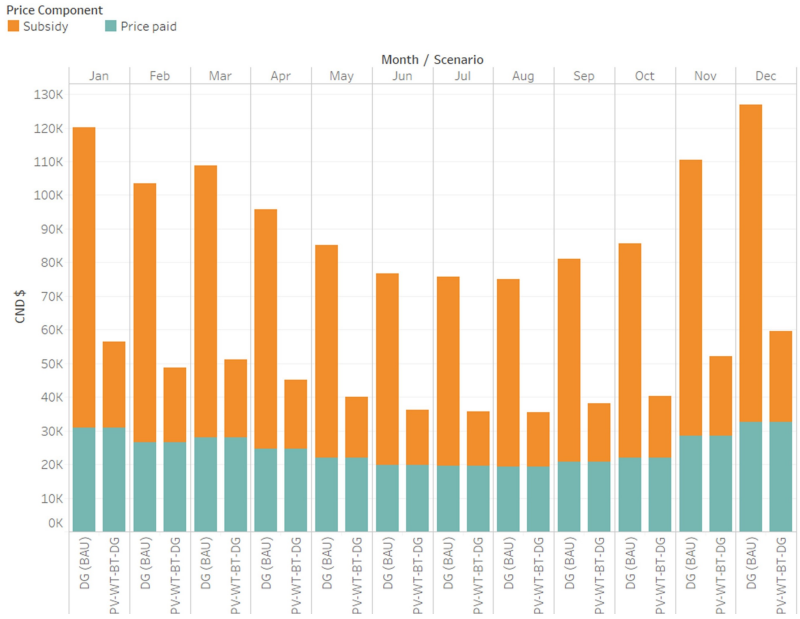

Figure 23: Comparative estimate of cost of energy for Sachs Harbour using diesel generator as its only source of power and the proposed hybrid microgrid system consists of wind, solar PV, battery storage and diesel generator.

The percentage error equation implemented in validating the results of the model is in Eq. 20.

$$\%Error = \frac{|HOMER - MINES|}{|MINES|} \tag{20}$$

For comparison, one point in the Pareto front in Fig. 18 was chosen. For example, the components of the solution with the lowest $LCOE$ under LFOS was extracted and simulated in HOMER. Results in Table 14 show that the difference is negligible between the two energy modeling tools. As well, it implicitly validates the optimization algorithm since the simulation process is linked to the GA as shown in Fig. 4. This validation proves that the model can be used in sizing individual components of the hybrid system on a more robust fashion. In addition, the multi-objective approach implemented in the study is more applicable in examining the complex trade-offs of priorities in designing energy system for an Arctic community or remote areas elsewhere.

4. Conclusion

In this work, a study was completed looking at alternatives in displacing diesel for power generation among Arctic communities in Canada. Solution diversity – as implemented in a multi-objective optimization approach – was established to be a research gap among recent energy studies done in an Arctic environment. Hence, MINES was proposed in order to investigate the complex trade-offs in designing a microgrid power system. A metaheuristic algorithm, specifically GA, was employed in the model as it can solve different combinatorial optimization problems and it can handle non-linearities as compared to classical optimization methods such as MILP which is rarely used for handling MOP.

Through GA, various components of the microgrid system were optimally sized. It was demonstrated with a case study on Sachs Harbour, the Northernmost region of the NWT. From the optimization process, a fully hybrid PV-WT-BT-DG-CONV has been proposed. The Pareto front confirmed the expected trend of the energy system: as $fuel_{cons}$ decreases, the system's $LCOE$ increases due to the integration of renewables and the BT storage, displacing diesel power in the energy mix. Three points on the Pareto front were analyzed focusing on solutions with minimum $LCOE$, maximum $LCOE$ and a point at the middle of the curve which was established to be a trade-off point. The three solutions of interest follow an $LPSP$ of 0% to ensure that the demand was met every timestep. A RE_{pen} above 70% was observed with wind having the largest share of power in the system. This reflects the excellent wind resource in the region and its technical viability.

The system with the lowest $LCOE$ in the Pareto front has a projected $LCOE$ of 52 CND cents/kWh versus an $LCOE$ of 111 CND cents/kWh for a diesel-only scenario (business-as-usual). The proposed hybrid system was also estimated to displace 675 MWh/yr of energy from diesel and it save 353,407 L/yr of fuel. Power dispatch laws were also found to greatly affect the overall optimized system configuration, particularly the performance of the generator as a back-up source of power.

The robustness of the results of the model were investigated by performing system failure simulation of each component of the hybrid system. It was highlighted that the DG is the most critical component in the operation of the microgrid. Failure of all other system components, on the other hand, is not crucial in maintaining supply reliability ($LPSP = 0\%$) but will increase fuel consumption to compensate unavailability of other component in the microgrid to produce power. The results show that multiple system configurations are viable and the model giving more flexibility in the decision making process of the communities.

The application of energy modeling in giving insights to policy makers has been highlighted. With the proposed modeling tool, decision makers can weigh pros and cons in upgrading current diesel facilities in the North versus increasing their investments for RE projects in the future. For example, it was shown that the optimal HRES resulted in a 70% cost reduction in the government subsidy budget for the community of Sachs Harbour. Such savings can then be allocated to increasing the uptake of RE in the community for the future. Another potential policy application of MINES is in defining the appropriate carbon price in the NWT. The tool is also flexible beyond the specific energy situation for different Arctic communities. The objective functions, constraints and other variables in the model can be altered, and policy insights can be framed from the quantitative model outputs.

To justify reliability of the simulation results, the proposed model was validated against HOMER and negligible percentage error was found between the two tools. The validation also implicitly validated the employed GA approach since the simulation and optimization algorithms were interlinked in the discussed methodology of this research.

Overall, the proposed model constitutes a useful energy modeling platform in solving challenges relating to energy affordability, environmental emissions and energy security in the North and other remote communities within and beyond Canada. Ultimately, through research and community engagement that stem from critical empathy, respect and reciprocity, the energy model framework is capable of quantifying project risk and performance will be used to help Indigenous communities return to more harmonious coexistence with nature to ensure their continued economic viability and quality of life.

The next stage of this research project is to expand the application of MINES by integrating heat with electrical load in the energy system in the Arctic and other remote communities. The authors are also working directly with WWF to have a holistic investigation in the energy situation in the Arctic by studying both the supply (energy resources) side and the demand aspect (energy conservation and efficiency measures) of various remote communities in the region.

Acknowledgement

Funding for this work was provided by Polar Knowledge Canada and the Marine Environmental Observation, Prediction and Response Network. Authors would also like to acknowledge support from the Government of Northwest Territories and Northwest Territories Power Corporation by providing actual electrical load and wind data which served as vital inputs for the project. Marvin Quitoras acknowledges the financial support from Mitacs Canada.

References

[1] Standing Senate Committee on Energy Environment and Natural Resources, Powering Canada's Territories, Technical Report, 2014.

[2] Pembina Institute, Leading Canada's transition to clean energy, 2019. URL: `https://www.pembina.org/`.

[3] Pembina Institute, Diesel, renewables, and the future of Canada's remote communities, 2019. URL: `https://www.pembina.org/blog/remote-microgrids-intro`.

[4] High Commission of Canada in the United Kingdom, The Canadian Arctic, 2018. URL: https://www.canadainternational.gc.ca/united{_}kingdom-royaume{_}uni/bilateral{_}relations{_}bilaterales/arctic-arctique.aspx?lang=eng.

[5] Government of Canada, The Paris Agreement, 2018. URL: https://www.canada.ca/en/environment-climate-change/services/climate-change/paris-agreement.html.

[6] R. Letzter, 2016 was the worst year ever in the Arctic, 2016. URL: https://www.businessinsider.com/arctic-warming-twice-fast-planet-2016-12.

[7] P. K. Quinn, T. S. Bates, E. Baum, N. Doubleday, A. M. Fiore, M. Flanner, A. Fridlind, T. J. Garrett, D. Koch, S. Menon, D. Shindell, A. Stohl, S. G. Warren, Short-lived pollutants in the Arctic: Their climate impact and possible mitigation strategies, Atmospheric Chemistry and Physics 8 (2008) 1723–1735.

[8] Environment and Natural Resources, Spills, 2019. URL: https://www.enr.gov.nt.ca/en/spills.

[9] The Narwhal, How can Canada's North get off diesel?, 2019. URL: https://thenarwhal.ca/how-canadas-north-get-off-diesel/.

[10] S. Shankman, Shipping's Heavy Fuel Oil Puts the Arctic at Risk. Could It Be Banned?, 2018. URL: https://insideclimatenews.org/.

[11] M. S. Gearon, D. F. McCay, E. Chaite, S. Zamorski, D. Reich, J. Rowe, D. Schmidt-Etkin, SIMAP Modelling of Hypothetical Oil Spills in the Beaufort Sea for World Wildlife Fund (WWF), Technical Report, 2014.

[12] CanmetENERGY, Energy Policy Context and Market Characterization for the Development of a Northern Communities Energy Technology Intervention Strategy, Technical Report September, 2015.

[13] Government of Canada (National Energy Board), Market Snapshot: Explaining the high cost of power in northern Canada, 2017. URL: https://www.neb-one.gc.ca/nrg/ntgrtd/mrkt/snpsht/2017/02-03hghcstpwr-eng.html?=undefined{&}wbdisable=true.

[14] D. Levin, Ice Roads Ease Isolation in Canada's North, but They're Melting Too Soon, 2017. URL: https://www.nytimes.com/2017/04/19/world/canada/ice-roads-ease-isolation-in-canadas-north-but-theyre-melting-too-soon.html.

[15] L. D. Bello, The Arctic is warming twice as fast as the rest of the globe, 2017. URL: https://futurism.com/the-arctic-is-warming-twice-as-fast-as-the-rest-of-the-globe.

[16] M. Biberacher, Modelling and optimisation of future energy system using spatial and temporal methods. Dissertation, Ph.D. thesis, University of Augsburg, 2004.

[17] International Energy Agency, RE-ASSUME : A decision maker's guide to evaluating energy scenarios modeling and assumptions, Technical Report June, 2013.

[18] I. Das, C. Canizares, Fuelling change in the arctic - Phase II (Feasibility studies on selected communities of Nunavut and Northwest Territories), Technical Report, World Wildlife Fund, Waterloo Institute for Sustainable Energy, 2016.

[19] HOMER Energy, HOMER Pro, 2019. URL: https://www.homerenergy.com/products/pro/index.html.

[20] I. Kim, J. A. James, J. Crittenden, The case study of combined cooling heat and power and photovoltaic systems for building customers using HOMER software, Electric Power Systems Research 143 (2017) 490–502.

[21] R. Sen, S. C. Bhattacharyya, Off-grid electricity generation with renewable energy technologies inIndia: An application of HOMER, Renewable Energy 62 (2014) 388–398.

[22] I. Prasetyaningsari, A. Setiawan, A. A. Setiawan, Design optimization of solar powered aeration system for fish pond in Sleman Regency, Yogyakarta by HOMER software, Energy Procedia 32 (2013) 90–98.

[23] O. Hafez, K. Bhattacharya, Optimal planning and design of a renewable energy based supply system for microgrids, Renewable Energy 45 (2012) 7–15.

[24] L. Montuori, M. Alcázar-Ortega, C. Álvarez-Bel, A. Domijan, Integration of renewable energy in microgrids coordinated with demand response resources: Economic evaluation of a biomass gasification plant by Homer Simulator, Applied Energy 132 (2014) 15–22.

[25] W. M. Amutha, V. Rajini, Cost benefit and technical analysis of rural electri fication alternatives in southern India using HOMER, Renewable and Sustainable Energy Reviews 62 (2016) 236–246.

[26] P. Tozzi, J. H. Jo, A comparative analysis of renewable energy simulation tools: Performance simulation model vs. system optimization, Renewable and Sustainable Energy Reviews 80 (2017) 390–398.

[27] H. K. Ringkjøb, P. M. Haugan, I. M. Solbrekke, A review of modelling tools for energy and electricity systems with large shares of variable renewables, Renewable and Sustainable Energy Reviews 96 (2018) 440–459.

[28] D. Connolly, H. Lund, B. V. Mathiesen, M. Leahy, A review of computer tools for analysing the integration of renewable energy into various energy systems, Applied Energy 87 (2010) 1059–1082.

[29] M. Ming, R. Wang, Y. Zha, T. Zhang, Multi-Objective Optimization of Hybrid Renewable Energy System Using an Enhanced Multi-Objective Evolutionary Algorithm, Energies 10 (2017) 674.

[30] A. Konak, D. W. Coit, A. E. Smith, Multi-objective optimization using genetic algorithms: A tutorial, Reliability Engineering and System Safety 91 (2006) 992–1007.

[31] D. B. Nelson, M. H. Nehrir, C. Wang, Unit sizing and cost analysis of stand-alone hybrid wind/PV/fuel cell power generation systems, Renewable Energy 31 (2006) 1641–1656.

[32] B. S. Borowy, Z. M. Salameh, Methodology for optimally sizing the combination of a battery bank and PV array in a Wind/PV hybrid system, IEEE Transactions on Energy Conversion 11 (1996) 367–373.

[33] A. Hadj Arab, F. Chenlo, M. Benghanem, Loss-of-load probability of photovoltaic water pumping systems, Solar Energy 76 (2004) 713–723.

[34] J. H. Lucio, R. Valdés, L. R. Rodrí guez, Loss-of-load probability model for stand-alone photovoltaic systems in Europe, Solar Energy 86 (2012) 2515–2535.

[35] R. Dufo-López, J. L. Bernal-Agustín, Multi-objective design of PV-wind-diesel-hydrogen-battery systems, Renewable Energy 33 (2008) 2559–2572.

[36] S. Abedi, A. Alimardani, G. B. Gharehpetian, G. H. Riahy, S. H. Hosseinian, A comprehensive method for optimal power management and design of hybrid RES-based autonomous energy systems, Renewable and Sustainable Energy Reviews 16 (2012) 1577–1587.

[37] A. R. Prasad, E. Natarajan, Optimization of integrated photovoltaic-wind power generation systems with battery storage, Energy 31 (2006) 1607–1618.

[38] S. Diaf, D. Diaf, M. Belhamel, M. Haddadi, A. Louche, A methodology for optimal sizing of autonomous hybrid PV/wind system, Energy Policy 35 (2007) 5708–5718.

[39] Y. Himri, A. Boudghene Stambouli, B. Draoui, S. Himri, Techno-economical study of hybrid power system for a remote village in Algeria, Energy 33 (2008) 1128–1136.

[40] R. Baños, C. Gil, B. Paechter, J. Ortega, A hybrid meta-heuristic for multi-objective optimization: MOSATS, Journal of Mathematical Modelling and Algorithms 6 (2007) 213–230.

[41] S. Upadhyay, M. P. Sharma, Selection of a suitable energy management strategy for a hybrid energy system in a remote rural area of India, Energy 94 (2016) 352–366.

[42] B. Jyoti Saharia, H. Brahma, N. Sarmah, A review of algorithms for control and optimization for energy management of hybrid renewable energy systems, Journal of Renewable and Sustainable Energy 10 (2018) 053502.

[43] T. Tezer, R. Yaman, G. Yaman, Evaluation of approaches used for optimization of stand-alone hybrid renewable energy systems, Renewable and Sustainable Energy Reviews 73 (2017) 840–853.

[44] O. Erdinc, M. Uzunoglu, Optimum design of hybrid renewable energy systems: Overview of different approaches, Renewable and Sustainable Energy Reviews 16 (2012) 1412–1425.

[45] M. S. Mahbub, M. Cozzini, P. A. Østergaard, F. Alberti, Combining multi-objective evolutionary algorithms and descriptive analytical modelling in energy scenario design, Applied Energy 164 (2016) 140–151.

[46] P. E. Campana, Z. Yang, L. Anders, L. Hailong, Y. Jinyue, An Open-source Platform for Simulation and Optimization of Clean Energy Technologies, Energy Procedia 105 (2017) 946–952.

[47] H. Yang, W. Zhou, L. Lu, Z. Fang, Optimal sizing method for stand-alone hybrid solar-wind system with LPSP technology by using genetic algorithm, Solar Energy 82 (2008) 354–367.

[48] M. Schoenauer, K. Deb, G. Rudolph, X. Yao, E. Lutton, J. J. Merelo, H.-P. Schwefel, Parallel Problem Solving from Nature - PPSN VI, 2000.

[49] M. Nemati, M. Braun, S. Tenbohlen, Optimization of unit commitment and economic dispatch in microgrids based on genetic algorithm and mixed integer linear programming, Applied Energy 210 (2018) 944–963.

[50] Z. I. Id, N. Javaid, S. Iqbal, S. Aslam, Z. A. Khan, A Domestic Microgrid with Optimized Home Energy Management System, Energies (2018) 1–39.

[51] Government of Northwest Territories, 2012 Northwest Territories Energy Charrette, Technical Report January, 2013.

[52] M. R. D. Quitoras, M. L. S. Abundo, L. A. M. Danao, A techno-economic assessment of wave energy resources in the Philippines, Renewable and Sustainable Energy Reviews 88 (2018) 68–81.

[53] Natural Resources Canada, Reducing diesel energy in rural and remote communities, 2019. URL: `https://www.nrcan.gc.ca/climate-change/green-infrastructure-programs/reducing-diesel-energy-rural-and-remote-communities/20542`.

[54] R. Ramakumar, I. Abouzahr, K. Ashenayi, A knowledge-based approach to the design of integrated renewable energy systems, IEEE Transactions on Energy Conversion 7 (1992) 648–659.

[55] J. J. Roberts, A. Marotta Cassula, J. L. Silveira, E. da Costa Bortoni, A. Z. Mendiburu, Robust multi-objective optimization of a renewable based hybrid power system, Applied Energy 223 (2018) 52–68.

[56] P. E. Campana, S. J. Quan, F. I. Robbio, A. Lundblad, Y. Zhang, T. Ma, B. Karlsson, J. Yan, Optimization of a residential district with special consideration on energy and water reliability, Applied Energy 194 (2016) 751–764.

[57] J. Duffie, W. Beckman, Solar Engineering of Thermal Processes, fourth edi ed., John Wiley & Sons, Inc. All, 2013.

[58] D. G. Eras, S. A. Klein, J. A. Duffle, Estimation of the diffuse radiation fraction for hourly, daily and monthly-average global radiation 28 (1982).

[59] J. J. Roberts, A. A. Mendiburu Zevallos, A. M. Cassula, Assessment of photovoltaic performance models for system simulation, Renewable and Sustainable Energy Reviews 72 (2017) 1104–1123.

[60] P. Jain, Wind Energy Engineering, McGraw-Hill Companies, Inc., New York, 2011. URL: www.google.com.

[61] T. Burton, N. Jenkins, D. Sharpe, E. Bossanyi, Wind Energy Handbook, second edi ed., John Wiley & Sons, Ltd, 2011. doi:10.1007/s007690000247. arXiv:arXiv:1011.1669v3.

[62] E. S. Sreeraj, K. Chatterjee, S. Bandyopadhyay, Design of isolated renewable hybrid power systems, Solar Energy 84 (2010) 1124–1136.

[63] J. F. Manwell, G. Jon, Lead acid battery storage model for hybrid energy systems 50 (1993) 399–405.

[64] E. J. Hoevenaars, C. A. Crawford, Implications of temporal resolution for modeling renewables-based power systems, Renewable Energy 41 (2012) 285–293.

[65] M. Matthew, Assessing the operational robustness of the HOMER model for Marine Corps use in expeditionary environments, Ph.D. thesis, Naval Postgraduate School, 2014.

[66] Northwest Territories Tourism, Sachs Harbour, 2019. URL: https://spectacularnwt.com/destinations/western-arctic/sachs-harbour.

[67] Meteonorm, Meteonorm, 2019. URL: https://meteonorm.com/.

[68] J. L. Sweeney, Modeling for Insights , not Numbers : the Experiences of the Energy Modeling Forum 1, OMEGA 10 (1982) 449–462.

[69] O. Williams, Sachs Harbour to receive new $10M diesel power plant, 2019. URL: https://cabinradio.ca/13683/news/economy/sachs-harbour-to-receive-new-10m-diesel-power-plant/.

[70] Government of the Northwest Territories, Implementing Pan-Canadian Carbon Pricing in the Northwest Territories, Technical Report July, 2017.

Nomenclature

BAU Business as Usual
BT Battery
CCOS Cycle Charging Operation Strategy
CONV Converter
DG Diesel Generator
GA Genetic Algorithm
HOMER Hybrid Optimization of Multiple Energy Resources
HRES Hybrid Renewable Energy System
KiBaM Kinetic Battery Model
LFOS Load Following Operation Strategy
MILP Mixed Integer Linear Programming
MINES Multi-objective INtegrated Energy System
MOP Multi Objective Problem
NOCT Nominal Operating Cell Temperature
NTPC Northwest Territories Power Corporation
NWT Northwest Territories
PV Photovoltaic
RE Renewable Energy
STC Standard Test Conditions
WT Wind Turbine
WWF World Wildlife Fund
α Wind power law exponent
α_p Temperature coefficient of power
$\bar{U}$ Annual mean wind speed
η_{gen} Wind turbine generator efficiency
$\eta_{mp,STC}$ Maximum power point efficiency of PV under STC
Γ Complete gamma function
ρ_a Air density
$\tau\alpha$ Effective transmittance-absorptance product of PV
A Rotor area of the wind turbine
c Scale parameter
C_p Wind power coefficient
c_{BT} Fraction of capacity that may hold available charge of BT
CC Capital cost
DG_{LF} Load factor of DG
EF Emission factor
$F(u)$ Percent of time hourly mean speed exceeds u
F_0 Fuel curve intercept coefficient
F_1 Fuel curve slope coefficient
f_{pv} PV derating factor
$fuel_{cons}$ Fuel consumption
GHI Global Horizontal Irradiance
$LOLP$ Loss of Load Probability
$LPSP$ Loss of Power Supply Probability
n Life of the energy system in years
N_{BT} Number of BT in the storage bank
NPC Net Present Cost
NPV Net Present Value
$O\&M$ Operations and maintenance costs
P_w Power output of the WT
P_{batt} Power stored from the BT
$P_{deficit}$ Insufficient supply of power from the power sources
$P_{DG,r}$ Rated capacity of DG
P_{DG} Power produced by DG
P_{excess} Excess electricity
P_{gen} Overall power generated from the system
P_{pv} Solar PV generation
P_{RE} Power produced by RE
$P_{w,r}$ Rated power output of the WT
POA Incident irradiance
POA_{NOCT} Solar radiation at which NOCT is defined
POA_{STC} Incident irradiance at STC
q_0 Stored energy
$q_{1,0}$ Available charge at the beginning of the timestep
q_1 Available charge at the end of the timestep
$q_{2,0}$ Bound charge at the beginning of the timestep
q_2 Bound charge at the end of the timestep
Q_{LT} Lifetime throughput of a single storage
q_{max} Maximum capacity of the BT
Q_{thrpt} Annual storage throughput
r Discount rate
$R_{BT,f}$ Storage float life
R_{BT} Battery bank life
RE_{pen} RE penetration
S Salvage value
SOC State of charge of the battery
SOC_{sp} Set point state of charge
T Overall time period considered
t Time
$T_{a,NOCT}$ Ambient temperature at which NOCTis defined
T_a Ambient temperature
$T_{c,NOCT}$ Nominal operating cell temperature

Table 1: Number of remote communities in Northern territories with their corresponding primary sources of electricity generation [1].

Source	Yukon	NWT	Nunavut
Diesel	5	23	25
Hydro	16	9	0
Natural gas	0	2	0

Table 2: Common objective functions in optimizing HRES according to literature.

Classification	Objective function	References
System reliability	Loss of Power Supply Probability ($LPSP$)	[31, 32]
	Loss of Load Probability ($LOLP$)	[33, 34]
System cost	Net Present Value (NPV)	[35, 36]
	Levelised Cost of Energy ($LCOE$)	[37, 38]
	Life Cycle Cost (LCC)	[39, 37]
Environmental	Fuel emissions	[29, 39]

Table 3: GA configuration parameters.

Parameter	Description
Algorithm	Variant of NSGA II [48]
Generations	200
Population	100
Crossover function	Heuristic
Crossover rate(%)	90
Mutation function	Non-uniform
Tournament size	2

Table 4: Emission factors in evaluating HRES [55].

Component	Indirect EF [1]		Direct EF [2]	
PV	0.059	$kgCO_2eq/kWh$	-	-
WT	0.02	$kgCO_2eq/kWh$	-	-
CONV	42.835	$kgCO_2eq/kW$	-	-
BT	59.42	$kgCO_2eq/kWh$	-	-
DG	454.293	$kgCO_2eq/kW$	2.64	$kgCO_2eq/L$
Diesel fuel	0.530	$kgCO_2eq/L$	-	-

[1] Emissions generated during the manufacturing, transportation and disposal stages.

[2] Emissions generated during the operation stage.

Table 5: Dimension of the discrete variables in the optimization algorithm.

Parameter	Value
WT quantity	0 - 500
WT capacity (kW)	95,95,100,100
PV quantity	0 - 500
PV capacity (kW)	15,25,20,25.025
BT quantity	0 - 500
BT capacity (kWh)	55,13.9,7.37,9.24
DG quantity	0 - 100
DG capacity (kW)	300,320,225,150
CONV quantity	0 - 10
CONV capacity (kW)	200,250,270,300
Operation strategy	LFOS and CCOS

Table 6: Solar PV parameters used in the simulation.

Parameter	Unit	Values per technology type			
		1	2	3	4
Manufacturer	-	Generic	Schneider Electric	Schneider Electric	Huawei
f_{pv}	%	80	85	85	96
α_p	%/°C	-0.44	-0.41	-0.41	-0.41
$\eta_{mp,STC}$	%	14.70	17.30	17.30	17.30
Lifetime	years	10	25	25	25

Table 7: Wind turbine parameters used in the simulation.

Parameter	Unit	Values per technology type			
		1	2	3	4
Manufacturer	-	XANT	Northern Power	XANT	Northern Power
Rated power	kW	95	95	100	100
Hub height	m	38	37	31.8	30
Lifetime	years	20	20	20	20

Table 8: Battery storage parameters used in the simulation.

Parameter	Unit	Values per technology type			
		1	2	3	4
Manufacturer	-	Generic	Rolls/Surrette	BAE Batterien GmbH	BAE Batterien GmbH
Nominal capacity	kWh	55	13.9	7.37	9.24
Nominal voltage	V	720	2	2	2
q_{max}	Ah	76.4	6950	3.68	4620
c_{BT}	-	0.927	0.267	0.369	0.355
k_{BT}	1/h	0.989	0.385	0.832	0.869
Roundtrip %	%	97	80	90	90
SOC_{min}	%	30	30	30	30
Q_{thrpt}	kWh/yr	240,000	19,434.10	7,728	9,744
$R_{BT,f}$	years	20	20	20	20

Table 9: Diesel generator parameters used in the simulation.

Parameter	Unit	Values per technology type			
		1	2	3	4
Manufacturer	-	Generic	Generic	Generic	Generic
Rated capacity	kWh	300	320	225	150
F_0	$L/h/kW_{rated}$	0.08145	0.08145	0.08145	0.08145
F_1	L/h/kW	0.246	0.246	0.246	0.246
c_{BT}	-	0.927	0.267	0.369	0.355
DG_{LF}	%	30	30	30	30
Lifetime	hours	15,000	15,000	15,000	15,000

Table 10: Converter parameters used in the simulation.

Parameter	Unit	Values per technology type			
		1	2	3	4
Manufacturer	-	Generic	Generic	Generic	Generic
Rated capacity	kW	200	250	270	300
Inverter %	%	95	95	95	95
Relative capacity [1]	%	100	100	100	100
Rectifier %	%	90	90	90	90
Lifetime	years	20	20	20	20

[1] Relative capacity of the rectifier in relation to the inverter .

Table 11: Configuration characteristics of the three solutions of interest determined from the Pareto front.

Parameter	Unit	Optimization results		
		Min. $LCOE$ and Max. $fuel_{cons}$	Trade-off Point	Max. $LCOE$ and Min. $fuel_{cons}$
PV	kW	100 (25kW x 4)	500 (25kW x 20)	175 (25kW x 7)
WT	kW	190 (95kW x 2)	190 (95kW x 2)	285 (95kW x 3)
BT	kWh	4,481.4 (9.24kWh x 485)	4,592 (9.24kWh x 497)	4,462 (9.24kWh x 483)
DG	kW	225 (225kW x 1)	225 (225kW x 1)	225 (225kW x 1)
CONV	kW	250 (250kW x 1)	250 (250kW x 1)	250 (250kW x 1)
Operation Strategy	-	CCOS	CCOS	CCOS
P_{pv}	kWh	81,457	407,285	142,550
P_w	kWh	818,800	823,921	1,235,882
$P_{BT,out}$	kWh	396,062	322,482	274,602
$P_{BT,in}$	kWh	393,032	319,610	272,550
P_{DG}	kWh	356,400	299,250	226,800
$LPSP$	%	0	0	0
RE_{pen}	%	71.64	80.45	85.87
P_{excess}	%	9.14	26.08	29.94
$fuel_{cons}$	L/yr	116,703	97,989	74,266
$CO_{2\,emissions,life\,cycle}$	tCO $_{2\text{-eq}}$/yr	770	736	646
CC	CND $	5,023,520	6,535,030	7,603,810
$LCOE$	CND $/kWh	0.522406	0.575872	0.61342
LCC	CND $	9,580,800	10,561,300	11,250,000

Table 12: Projected annual diesel displaced and emission reductions with the lowest LCOE configuration in the Pareto front of each possible combination of the hybrid microgrid system.

System	Diesel displaced (MWh)	Diesel fuel saved (L)	Emission reductions ($tCO_{2\text{-eq}}$)	$LCOE$ (CND $/kWh)	LCC (CND $)
DG (BAU)	-	-	-	1.11	20,357,700
PV-BT-DG	291	227,568	460	0.60	10,975,500
PV-DG	339	220,279	719	0.74	13,377,800
PV-WTBT-DG	675	353,407	854	0.52	9,580,800
PV-WT-DG	606	266,055	800	0.83	15,165,300
WT-BT-DG	629	338,303	816	0.53	9,765,020
WT-DG	632	307,138	1,015	0.70	12,900,300

Table 13: Impact of system component failure in the overall performance of the fully hybrid (PV-WT-BT-DG) microgrid system.

Cause of system failure	$LPSP$ (%)	$LCOE$ (CND \$/kWh)	$fuel_{cons}$ (L/yr)	P_{DG} (kWh/yr)
No failure	-	0.52	116,703	356,400
DG	27.12	0.41	-	-
PV	-	0.53	132,028	403,200
WT	-	0.76	382,895	1,169,325
BT	-	0.75	199,753	444,362
CONV	-	1.2	414,280	1,031,471

Table 14: Validation of simulation results with HOMER.

Parameter	Unit	Simulation results		
		HOMER	MINES	% Error
P_{pv}	kWh	138,053	138,136	0.06%
P_w	kWh	825,181	818,800	0.78%
P_{DG}	kWh	266,633	271,093	1.65%
P_{excess}	%	12.84	12.51	2.57%
$fuel_{cons}$	L/yr	111,426	113,439	1.77%
SOC[1]	%	568,955	570,632	0.25%
CC	CND \$	5,179,598	5,179,600	0%
$LCOE$	CND \$/kWh	0.57610	0.56998	1.06%
LCC	CND \$	10,565,080	10,453,200	1.06%

[1] For the sake of comparison, SOC per timestep was summed up for one whole year and compared to HOMER.